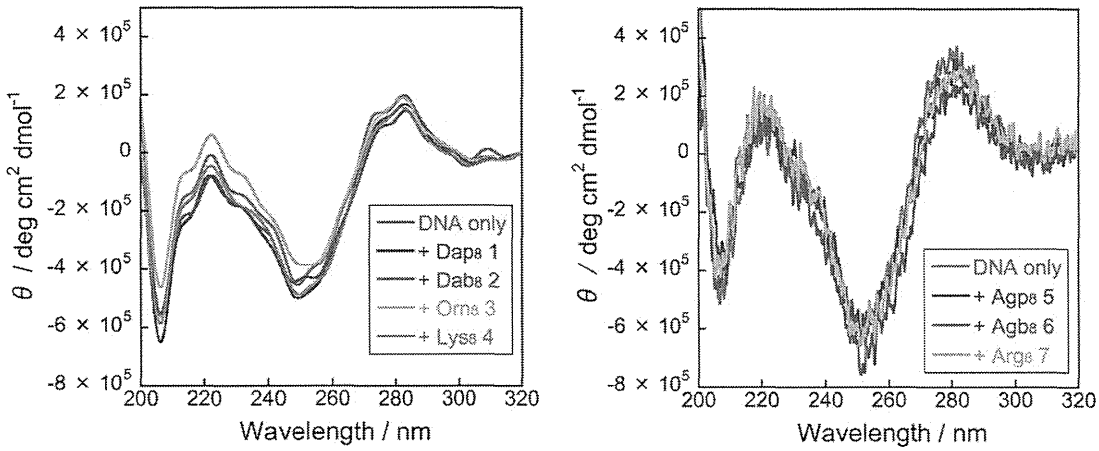

Figure 8. CD spectra of the DNA/DNA duplexes in the presence and absence of an equal amount of peptides **1–7** (at 20 °C, pH 7.0, 4 μM each of peptide and duplex).

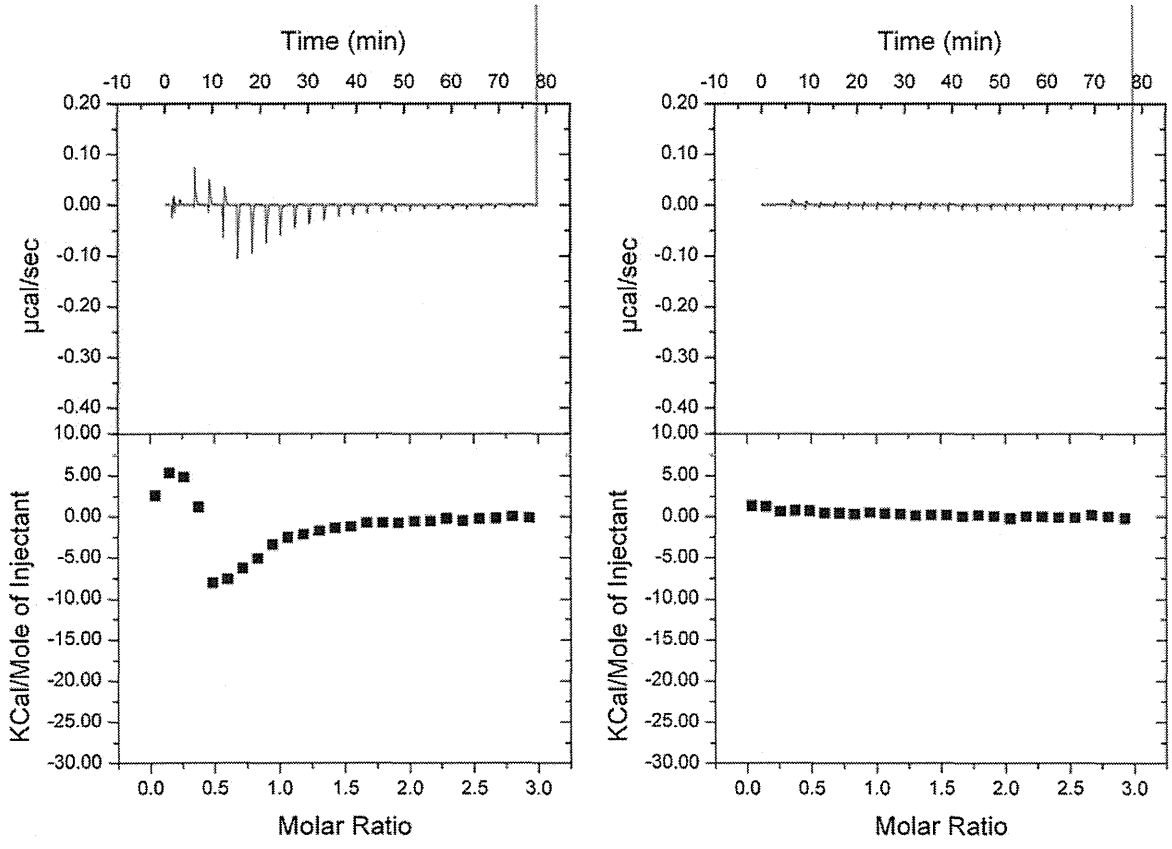

Figure 9. ITC profiles at 25 °C for titration of Dab_8 (**2**) into a solution of RNA/RNA duplex (left) and DNA/DNA duplex (right); each curve is the result of a 2.5 μl injection of 150 μM peptide. The duplex concentration was 10 μM in a 10 mM phosphate buffer with 100 mM NaCl at pH 7.0; corrected injection heat in the cases of RNA/RNA were plotted.

calcd for $[M+H]^+$ 1198.18; Found 1197.67. Compound **15**, TOF-MS *m/z* calcd for $[M+H]^+$ 1306.29; Found 1305.46.

3.2. Melting temperature (T_m) analysis

Absorbance versus temperature profile measurements were carried out in quartz cells with a 1 cm path length using an eight-sample cell changer. The variation in the UV absorbance with temperature was monitored at 260 nm. The temperature was scanned from 10 to 95 °C at a rate of 0.2 °C/min. The peptides were added after oligonucleotides were annealed. The samples were prepared as follows. The oligonucleotides were dissolved in a phosphate buffer (10 mM) containing NaCl (0.1 M) at pH 7.0. The solutions of oligonucleotides (4 μM) were first rapidly heated to 95 °C, left for 10 min, and then cooled to 10 °C at a rate of 1 °C/min. The equal amounts of peptides (final concn: 4 μM) were then added to the solution. The samples were left to equillbrate at the starting temperature for 30 min, the dissociation of the duplex was observed by heating the solution to 95 °C at a rate of 0.2 °C/min, and data points were collected at every 0.1 °C.

3.3. CD spectroscopy

All CD spectra were recorded at 20 °C. The following instrument settings were used: resolution, 0.1 nm; sensitivity, 10 mdeg; response, 4 s; speed, 10 nm/min; accumulation, 6.

3.4. Conditions for ITC experiments

The peptides and nucleic acid duplexes were dissolved in a 10 mM phosphate buffer containing 100 mM NaCl at pH 7.0. The peptide solutions (150 μM) were titrated into the nucleic acid duplex solutions (10 μM) at 25 °C. Each titration of peptide solution consisted of a preliminary 0.5 μl injection followed by 24 subsequent 1.5 μl additions, which were performed over 3 s periods at 120 s intervals. In the inhibition assays, the peptide solutions were titrated into the nucleic acid solution in the presence of 100 μM neomycin under the same conditions as described above.

4. Conclusion

We have synthesized a series of cationic oligopeptides by systematically changing the position of the cationic groups. On the basis of UV-melting analysis, CD spectrometry and ITC measurements, these cationic oligopeptides showed different tendencies for the stabilization of nucleic acid duplexes. Peptides with amino groups stabilized only RNA duplexes, while peptides with guanidino groups stabilized both RNA and DNA duplexes. In particular, Dab_8 (**2**) and Agp_8 (**5**) showed the highest T_m values among the series of peptides with the same cationic groups but different side chain length. These results suggest that the distance between the cationic groups, such as in Dab_8 (**2**) and Agp_8 (**5**), are well fitted to the distance between the phosphate groups in the major groove of RNA duplexes. Furthermore, peptides with alternate arrangements and those containing flexible amino acids did not stabilize the RNA duplexes. These results indicate that at least two consecutive sequences of Agp are necessary for effective binding of cationic oligopeptides to RNA duplexes. Therefore, given their unique properties, Dab_8 (**2**) and Agp_8 (**5**) will be useful as stabilizers of dsRNA-based nucleic acid drugs or new materials for their DDS.

Acknowledgments

We thank Professor Kohei Tsumoto (University of Tokyo) and Dr. Satoru Nagatoishi (University of Tokyo) for the ITC measurements and helpful discussions. This work was finally supported by KAKENHI and CREST, the Japan Science and Technology Agency.

Supplementary data

Supplementary data (data include CD spectra, UV melting profiles, and ITC profiles) associated with this article can be found, in the online version, at http://dx.doi.org/10.1016/j.bmc.2013.01.053.

References and notes

1. Fire, A.; Xu, S.; Montgomery, M. K.; Kostas, S. A.; Driver, S. E.; Mello, C. C. *Nature* **1998**, *391*, 806.
2. Watts, J. K.; Deleavey, G. F.; Damha, M. J. *Drug Discovery Today* **2008**, *13*, 842.
3. (a) Manoharan, M. *Biochim. Biophys. Acta* **1999**, *1489*, 117; (b) Cook, P. D. *Nucleosides Nucleotides* **1999**, *18*, 1141.
4. Eguchi, A.; Meade, B. R.; Chang, Y. C.; Fredrickson, C. T.; Williert, K.; Puri, N.; Dowdy, S. F. *Nat. Biotechnol.* **2009**, *27*, 567.
5. Prakash, T. P.; Allerson, C. R.; Vickers, T. A.; Sioufi, N.; Jarres, R.; Baker, B. F.; Swayze, E. E.; Griffey, R. H.; Bhat, B. *J. Med. Chem.* **2005**, *48*, 4247.
6. Francois, B.; Russell, R.; Murray, J. *Nucleic Acids Res.* **2005**, *33*, 5677.
7. Maris, C.; Dominguez, C.; Allain, F. H. *FEBS J.* **2005**, *272*, 2118.
8. (a) Nurtola, M.; Zaramella, S.; Yeheskiely, E.; Strömberg, R. *ChemBioChem* **2010**, *11*, 2606; (b) Wu, C. H.; Chen, Y. P.; Mou, C. Y.; Cheng, R. P. *Amino Acids* **2012**. http://dx.doi.org/10.1007/s00726-012-1357-0.
9. Iwata, R.; Sudo, M.; Nagafuji, K.; Wada, T. *J. Org. Chem.* **2011**, *76*, 5895.
10. Lemberg, M. K.; Martoglio, B. *Mol. Cell* **2002**, *10*, 735.
11. Futaki, S.; Suzuki, T.; Ohashi, W.; Yagami, T.; Tanaka, S.; Ueda, K.; Sugiura, Y. *J. Biol. Chem.* **2001**, *276*, 5836.
12. Kim, S. W.; Kim, N. Y.; Choi, Y. B.; Yang, J. M.; Shin, S. *J. Controlled Release* **2010**, *143*, 334.
13. Russell, A. L.; Williams, B. C.; Spuches, A.; Klapper, D.; Srouji, A. H.; Hicks, R. P. *Bioorg. Med. Chem.* **2012**, *20*, 1723.
14. Jones, S.; Daley, D. T.; Luscombe, N. M.; Berman, H. M.; Thornton, J. M. *Nucleic Acids Res.* **2001**, *29*, 943.
15. Mohamadi, F.; Richards, N. G. J.; Guida, W. C.; Liskamp, R.; Lipton, M.; Caufield, G.; Chang, G.; Hendrickson, T.; Still, W. C. *J. Comput. Chem.* **1990**, *143*, 334.
16. Ura, Y.; Leman, J.; Orgel, L. E.; Ghadiri, M. R. *Science* **2009**, *325*, 73.
17. See the Supplementary data.
18. Varani, L.; Spillantini, M. G.; Goedert, M.; Varani, G. *Nucleic Acids Res.* **2000**, *28*, 710.
19. *Fmoc Solid Phase Peptide Synthesis*; Chan, W. C., White, P. D., Eds.; Oxford University Press: New York, 2000. pp 42–76.
20. Xiao, S.; Fu, N.; Peckham, K.; Smith, B. D. *Org. Lett.* **2010**, *12*, 140.

HUMAN GENE THERAPY METHODS 23:119–127 (April 2012)

DOI: 10.1089/hgtb.2012.035

Intrathecal shRNA-AAV9 Inhibits Target Protein Expression in the Spinal Cord and Dorsal Root Ganglia of Adult Mice

Takashi Hirai,[1] Mitsuhiro Enomoto,[1] Akira Machida,[2] Mariko Yamamoto,[2] Hiroya Kuwahara,[2] Mio Tajiri,[2] Yukihiko Hirai,[3] Shinichi Sotome,[1] Hidehiro Mizusawa,[2] Kenichi Shinomiya,[1] Atsushi Okawa,[1] and Takanori Yokota[2]

Abstract

Gene therapy for neurological diseases requires efficient gene delivery to target tissues in the central and peripheral nervous systems. Although adeno-associated virus is one of the most promising vectors for clinical use against neurological diseases, it is difficult to get it across the blood–brain barrier. A clinically practical approach to using a vector based on adeno-associated virus to decrease the expression of a specific gene in both the central and the peripheral nervous system has yet to be established. Here, we analyzed whether upper lumbar intrathecal administration of a therapeutic vector incorporating adeno-associated virus and short-hairpin RNA against superoxide dismutase-1 bypassed the blood–brain barrier to target the spinal cord and dorsal root ganglia. The therapeutic vector effectively suppressed mRNA and protein expression of endogenous superoxide dismutase-1 in the lumbar spinal cord and dorsal root ganglia. Moreover, neither neurological side effects nor toxicity due to the incorporated short-hairpin RNA occurred after the injection. We propose that this approach could be developed into novel therapies for motor neuron diseases and chronic pain conditions, such as complex regional pain syndrome, through silencing of the genes responsible for pathologies in the spinal cord and dorsal root ganglia.

Introduction

The spinal cord is an important organ for sensory and motor signal processing and is an important anatomical target for neurological disorders, including inflammatory and demyelinating diseases, neurodegenerative diseases, traumatic injury, and neuropathic pain. The delivery of drugs to the spinal cord via systemic administration, such as oral ingestion, intravenous injection, and dermal application, encounters several challenges. Various types of gene therapy vectors have been developed for targeting the central nervous system (CNS). Intravenous injection of a vector based on adeno-associated virus (AAV) can deliver target genes to multiple organs, including the liver and skeletal and cardiac muscle (Mitchell *et al.*, 2000; Gregorevic *et al.*, 2004; Bish *et al.*, 2008). However, delivery of systemically administered AAV to the CNS via the blood–brain barrier has not yet been established, and to avoid systemic side effects, selective administration to the brain or spinal cord is required. Gene therapy trials for Parkinson's disease (Marks *et al.*, 2008), Canavan (Janson *et al.*, 2002), and Batten disease (Worgall *et al.*, 2008) have successfully involved direct brain injection of AAV vectors, but such an invasive method is limited in its application in common clinical practice.

RNA interference (RNAi) has emerged as a powerful tool to induce loss-of-function phenotypes through the posttranscriptional silencing of gene expression (Fire *et al.*, 1998; Dorn *et al.*, 2004). The RNAi pathway is initiated by the enzyme Dicer, which cleaves long, double-stranded RNAs into short (21- to 23-nucleotide) interfering RNA molecules (siRNAs) that mediate sequence-specific gene silencing (Mikami and Yang, 2005; Li *et al.*, 2008). Intraventricular (Senn *et al.*, 2005; Senechal *et al.*, 2007) and intrathecal administration (Luo *et al.*, 2005) of naked or lipid-encapsulated siRNA (Uno *et al.*, 2011) has been used to target the CNS. However, because they still show low transduction efficiencies, insufficient inhibition of gene expression, and short duration of therapeutic effects, these methods are unsuitable for treating chronic neurological disorders (Hassani *et al.*, 2005). To address these

[1]Department of Orthopedic Surgery, Graduate School, Tokyo Medical and Dental University, Tokyo 113–8519, Japan.
[2]Department of Neurology and Neurological Science, Graduate School, Tokyo Medical and Dental University, Tokyo 113–8519, Japan.
[3]Department of Biochemistry and Molecular Biology, Nippon Medical School, Bunkyo-ku, Tokyo 113–0022, Japan.

problems, therefore, viral delivery of short-hairpin RNA (shRNA) expression cassettes that support more efficient and long-lasting transduction into the target CNS is expected to be a promising delivery tool. Local administration methods, such as intramuscular, intrastriatal, and subcutaneous injections, for delivering the viral vector encoding the shRNA have been reported to inhibit target gene expression in mice (Rodriguez-Lebron *et al.*, 2005; Towne *et al.*, 2008; Fu *et al.*, 2009). However, intrathecal injection of shRNA-encoding viral vectors has not yet been documented to reduce the levels of mRNA and protein in the spinal cord and dorsal root ganglia (DRG). To this end, here we show that intrathecal delivery of the AAV-based vector shRNA-AAV9 to mice efficiently inhibited endogenous superoxide dismutase-1 (SOD1), which is ubiquitously expressed in neural tissues.

Materials and Methods

*Construction, production, and titration of anti-*SOD1 *shRNA AAV9 vector*

We prepared the anti-*SOD1* shRNA cassette as previously reported (Yokota *et al.*, 2004; Mayra *et al.*, 2011). The anti-*SOD1* shRNA cassette was cloned downstream of the human polymerase III (Pol III) U6 promoter in the AAV9 vector plasmid (Stratagene, La Jolla, CA). The silencing efficiency of the anti-*SOD1* shRNA sequence was verified using several cultured cell lines and transgenic mice expressing the anti-*SOD1* shRNA, as previously described (Federici *et al.*, 2011). A human growth hormone polyadenylation [hGH poly(A)] cassette (Stratagene) was inserted downstream of the shRNA sequence in the vector for vector titration by quantitative real-time PCR (Fig. 1). The recombinant viral vector was produced according to the three-plasmid transfection protocol and the calcium phosphate method, as previously reported (Hermens *et al.*, 1999).

Animals

All of the animal procedures were performed in accordance with protocols approved by the Animal Experiment Committee of Tokyo Medical and Dental University (Tokyo, Japan) (#81213). Eight-week-old female ICR mice weighing 25–35 g were given intrathecal injections. The animals were divided into two groups: the AAV-treated group (AAV; $n=9$) and the phosphate-buffered saline (PBS)-treated group (PBS; $n=9$). After having been given intraperitoneal injections of chloral hydrate (0.5 mg/g body weight) and ketamine hydrochloride (0.05 mg/g body weight), mice from both the AAV- and PBS-treated groups were placed in the prone position, and a partial laminectomy of the caudal portion of the second lumbar vertebra and the rostral portion of the third lumbar vertebra was performed. The dural matter was exposed and punctured with a 27-gauge needle. Subsequently a PE-10 tube was connected to a 10-μl Hamilton syringe and caudally inserted into the subarachnoid space between these two vertebrae. A volume of 10 μl (6×10^{12} vector genome per microliter) of either the shRNA-AAV9 vector targeting SOD1 or PBS was injected slowly over a 2-min period. After removal of the catheter, the incision was sutured, and the mice were maintained in the head-up position and allowed to recover on a heating pad. The body weights of the mice were measured every week. At 2 and 4 weeks after the injection, all of the mice were killed, and the lumbar spinal cord, lumbar DRG, cardiac muscle, liver, and quadriceps muscle were harvested for analysis. All animal experiments were performed in accordance with the ethical and safety guidelines for animal experiments of the Tokyo Medical and Dental University.

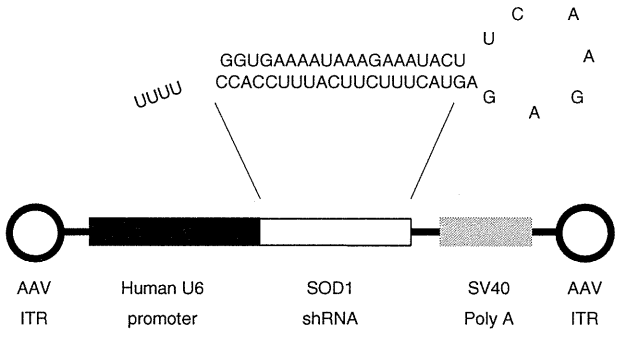

FIG. 1. Construction of the anti-*SOD1* shRNA AAV9 vector. The anti-*SOD1* shRNA expression AAV9 vector, including the anti-*SOD1* shRNA sequence located between the human polymerase III human U6 promoter and the hGH poly(A) cassette, is shown. AAV, adeno-associated virus; hGH, human growth hormone; ITR, inverted terminal repeat; shRNA, short-hairpin RNA; SOD1, superoxide dismutase-1; SV40, simian virus 40.

Measurement of mRNA reduction by quantitative RT-PCR

Total RNA was extracted from the harvested tissues, including the lumbar segment of the spinal cord, the lumbar DRG, cardiac muscle, liver, and the quadriceps muscle, using Isogen (Nippon Gene, Tokyo, Japan). The RNA samples obtained from the lumbar spinal cord were collected from the lumbar region located at the first to second vertebral level. The RNA samples obtained from the DRG consisted of three ganglia, including the fourth, fifth, and sixth lumbar DRG. The DNase I-treated total RNA (0.5 μg) was reverse transcribed, using SuperScript III reverse transcriptase (Invitrogen, Carlsbad, CA). The cDNA was amplified by the quantitative TaqMan system with a LightCycler 480 real-time PCR instrument (Roche, Basel, Switzerland), according to the manufacturer's protocol. The *SOD1* mRNA expression level in each tissue was measured with the following primers and probe: forward primer, 5′-GGTGCAGGGAACCATC-CA-3′; reverse primer, 5′-CCCATGCTGGCCTTCAGT-3′; and probe, 5′-AGGCAAGCGGTGAACCAGTTGTGTTG-3′. Primers for mouse transthyretin (TTR) were designed by Applied Biosystems (Foster City, CA). To normalize the RT-PCR values, the cDNA was also quantitatively amplified with the TaqMan primer and probe sets for glyceraldehyde-3-phosphate dehydrogenase (GAPDH; Applied Biosystems, Warrington, UK). The ratio of *SOD1* mRNA expression to that of GAPDH was calculated to estimate the shRNA silencing efficiency.

Northern blotting analysis of shRNA

RNA was obtained from the lumbar segment of the spinal cord and the lumbar DRG, which were harvested from the bilateral third to sixth lumbar DRG using mirVana (Ambion,

Austin, TX). Five micrograms of RNA derived from the spinal cord and 1 μg of RNA from the DRG were separated on 18% polyacrylamide–urea gels and transferred to Hybond-N+ membranes (GE Healthcare, Piscataway, UK). The blots were hybridized with a probe against the antisense sequence of the shRNA, and the probe sequence was 5′-GGTGGAAATGAAGAAAGTAC-3′. The probe was labeled with a DIG oligonucleotide 3′-end labeling 2nd generation kit (Roche, Penzberg, Germany), and the signal was visualized with a Gene Images CDP-Star detection kit (GE Healthcare).

microRNA expression by quantitative RT-PCR

The expression levels of ubiquitous microRNAs (miRNAs) were measured with miRNA sequence-specific primers (Applied Biosystems, Foster City, CA) and RT-PCR-based detection methodology. Briefly, 100 ng of miRNA collected from the lumbar DRG and spinal cord was reverse transcribed, using PrimeScript RT master mix (Takara Bio, Shiga, Japan) and subsequently amplified with a LightCycler 480 real-time PCR instrument (Roche, Basel, Switzerland). Small nucleolar RNA U6 was used as an endogenous control. The ratio of let-7 or miR-124 expression to that of U6 was calculated to estimate the shRNA silencing efficiency.

Western blotting

A sample from the lumbar spinal cord was collected between the first and second vertebrae, and the DRG sample was extracted from the third, fourth, and fifth lumbar DRG. These tissues were homogenized in cold homogenization buffer containing 0.1% sodium dodecyl sulfate (SDS), 1% sodium deoxycholate, 1% Triton X-100, and 1 *mM* phenylmethylsulfonyl fluoride together with a protein inhibitor cocktail (Roche, Penzberg, Germany). Five micrograms of extracted protein from each sample was mixed with Laemmli sample buffer (Bio-Rad, Hercules, CA), denatured at 37°C for 60 min, and separated on an SDS–15% polyacrylamide gel. The separated proteins were transferred to a polyvinylidene difluoride membrane (Bio-Rad) and were then incubated with specific primary antibodies, including a rabbit anti-SOD1 antibody (Stressgen Biotechnologies, Victoria, BC, Canada) and a mouse anti-GAPDH monoclonal antibody (Biodesign, Saco, ME). After incubation, the membranes were rinsed and incubated with a 0.1% solution of the horseradish peroxidase (HRP)-conjugated secondary antibodies, including goat anti-rabbit HRP IgG and goat anti-mouse HRP IgG (Thermo Science, Rockford, IL). The protein–antibody interactions were visualized with SuperSignal West Femto maximum sensitivity substrate (Thermo Science). The quantification of the band intensity was measured by Scion imaging (National Institutes of Health, Bethesda, MD). We calculated the relative protein expression levels in the lumbar spinal cord and DRG in the AAV-treated group as compared with those in the PBS-treated group.

Histological examinations

Mice were killed by transcardiac perfusion of PBS for 5 min at room temperature, followed by 4% paraformaldehyde (PFA) in PBS for 15 min at 4°C. After perfusion, the lumbar spinal cord and DRG were immediately removed and postfixed in 4% PFA in PBS at 4°C overnight. After fixation, the samples were transferred to PBS containing 30% sucrose and dehydrated for 3 days. The tissues were then embedded in paraffin or low melting temperature agarose (BM Equipment, Tokyo, Japan) in PBS. Ten-micron paraffin sections of the lumbar spinal cord were processed for hematoxylin and eosin and Nissl staining. Frozen sections approximately 20 μm thick from the fifth lumbar (L5) DRG and the spinal cord at the first lumbar vertebral level from mice in each group were incubated for 30 min at room temperature in a blocking solution (5% normal goat serum). The sections were then incubated with a rabbit polyclonal anti-SOD1 antibody (diluted 1:1000; Stressgen Biotechnologies) for 24 hr at 4°C. After incubation, the sections were washed and incubated for 30 min at room temperature with the biotinylated secondary antibody (diluted 1:200; Vector Laboratories, Burlington, ON, Canada) in 0.5% horse serum. The sections were then incubated with ABC reagent (Vector Laboratories) for 30 min, followed by incubation with peroxidase substrate solution for 2 min. After washing, the tissue sections were counterstained with hematoxylin for 1 min.

Rotarod test

The locomotive test was performed with an accelerating Rotarod (Ugo Basile Biological Research Apparatus, Varese, Italy). Mice from both groups were placed on 3-cm rods and were subjected to four trials each day for 4 days. Each trial lasted up to 10 min, and the length of time that the animals could balance on the rod without falling was recorded.

Sensory behavioral tests

The animals were placed in Plexiglas boxes, which were 9.5×21×25 cm in size, to become acclimated to the testing environment. These boxes were then placed on an elevated perforated plastic surface for a minimum of 30 min before all behavioral tests (Hargreaves *et al.*, 1988). A blind observer conducted the behavioral testing.

Tactile threshold. Mechanical sensitivity was measured by applying a series of calibrated von Frey filaments (0.02–8 g) to the plantar aspect of the hind paw. Each filament was applied once to each mouse. Beginning with the 1-g filament, each filament was applied perpendicular to the hind paw for 4–6 sec. A brisk withdrawal of the hind paw indicated a positive response, and the lack of withdrawal indicated a negative response. This filament testing was repeated a maximum of two additional times, and at least two positive responses in three to the filament indicated an overall positive response. If the mouse demonstrated an overall positive response, the next lower force filament was applied as described previously. If no overall positive response was observed (zero or one response in three), the next greater force filament was applied as described previously. Once the crossover threshold could be determined (i.e., from response to no response, or vice versa) the responses to the next five filaments were recorded to determine the median withdrawal threshold.

Response to acetone. Using a plastic tube connected to a 1-ml syringe, and without touching the skin, 100 μl of acetone was applied to the plantar surface of the foot. Acetone

was applied five times to each paw at an interval of at least 30 sec, and the number of brisk foot withdrawals in response to the acetone application was recorded.

Response to noxious heat stimulus. Responses to noxious radiant heat were determined by the Hargreaves method and the Ugo Basile plantar test apparatus. Mice were placed in a transparent plastic chamber on a glass floor and were allowed to acclimate for 30 min. The radiant heat source was placed under the glass floor directly beneath the hind paw. The intensity of the heat stimulus was set to 60 J. Withdrawal latencies were defined as the time between the activation of the heat source and hind paw withdrawal. Withdrawal resulted in the termination of the heat source. A time limit of 15 sec was used to prevent tissue damage. A 5-min interval between consecutive stimulations of the same hind paw was employed. Testing was performed five times on each side, and the latencies for each side were averaged.

Statistical analyses

All data are presented as means ± standard deviation (SD; $n=3$–5). We performed the statistical analysis by Student t test for comparisons between the two groups for all experiments, with the exception of the Rotarod test. For the Rotarod test, the average time of each group was calculated, and statistical significance was assessed by one-way analysis of variance. Significance was defined as p values less than 0.05.

Results

SOD1 mRNA and protein expression in the spinal cord and DRG after lumbar intrathecal administration of shRNA-AAV9

An shRNA-AAV9 vector targeting SOD1 was injected into the subarachnoid space at the second lumbar vertebra of mice to determine the ability of the vector to suppress the expression of SOD1 in the spinal cord and DRG. We first analyzed the efficiency with which *SOD1* mRNA was silenced in various tissues from mice in the AAV-treated group. Quantitative RT-PCR analysis showed that the expression of *SOD1* mRNA in the quadriceps, cardiac muscles, and liver of animals in the AAV-treated group was similar to that of mice that received PBS only (Fig. 2A). However, the level of *SOD1* mRNA in the lumbar spinal cord and DRG of mice in the AAV-treated group was about 60% lower than that in PBS-treated animals (Fig. 2B). These silencing effects in the lumbar spinal cord and lumbar DRG persisted for at least 4 weeks and tended to increase in a time-dependent manner (Fig. 2A). The knockdown effect was specific for the target gene (*SOD1*), given that the levels of other endogenous mRNAs, of GAPDH and TTR, did not change (Fig. 2B), suggesting that shRNA-AAV9 did not affect unrelated endogenous gene expression. Western blot analysis confirmed decreased SOD1 protein levels in the lumbar spinal cord and DRG of shRNA-AAV9–treated mice (Fig. 2C). Four weeks after injection of shRNA-AAV9, the mean level of SOD1 protein expression was 72% lower in the lumbar spinal cord and 68% lower in the lumbar DRG compared with the amounts in PBS-treated mice (Fig. 2D). Immunohistochemical analysis with anti-SOD1 antibody confirmed silencing of SOD1 within the lumbar spinal cord and DRG. The SOD1 immunoreactivity of the lumbar spinal cord and DRG was much lower in the AAV-treated group than in the PBS-treated group (Fig. 2E).

Robust delivery of shRNA-AAV9 to the lumbar spinal cord and DRG, and detection of siRNA derived from shRNA encoded by AAV9 in these tissues

To investigate whether shRNA-AAV9 was delivered to the lumbar spinal cord and DRG, we used Northern blotting to examine the expression of anti-*SOD1* shRNA in these tissues. The 54-nucleotide intact shRNA was not present, but a 21-nucleotide antisense strand of siRNA was detected in both tissues (Fig. 2F). This finding clearly indicated that the shRNA encoded by AAV9 was in fact delivered to the cytosol of target cells and that the expressed anti-*SOD1* shRNA was almost completely processed by Dicer.

Endogenous miRNA expression in the lumbar spinal cord and DRG after intrathecal injection of shRNA-AAV9

Because both RNA forms share intracellular machinery for their expression in mammalian cells, we sought to clarify whether overexpression of shRNA decreased the processing of endogenous miRNA (Grimm *et al.*, 2006; Rossi, 2008). To this end, we used quantitative RT-PCR to evaluate the expression levels of representative miRNAs (let-7 and miR-124) in the lumbar spinal cord and DRG. Expression levels of let-7 and miR-124 (Fig. 3A) were similar in PBS- and AAV-treated mice. These results indicate that the endogenous miRNA pathway was preserved in the lumbar spinal cord and DRG after injection of shRNA-AAV9.

Histological evaluations of the lumbar spinal cord and DRG

We histologically evaluated whether any anatomical abnormalities occurred in the lumbar spinal cord and DRG after shRNA-AAV9 injection. Hematoxylin and eosin staining of these tissues showed no inflammation, necrosis, or degenerative lesion formation (Fig. 3B). In addition, Nissl staining revealed no structural neuronal deterioration after injection of shRNA-AAV9 (Fig. 3B).

Body weight and locomotive and sensory functions

To assess the general health and motor and sensory functions of the hind limbs of mice after injection of PBS or shRNA-AAV9, we observed these animals for 2 to 4 weeks after treatment. Body weights of the mice in the AAV-treated group were similar to those in the PBS-treated group (Fig. 4A). In addition, accelerating Rotarod tests revealed no significant differences in motor function between the PBS- and AAV-treated mice (Fig. 4B). Furthermore, there were no significant differences between groups, either before or after treatment, according to the thermal (Fig. 4C), tactile (Fig. 4D), and acetone (Fig. 4E) tests.

Discussion

Successful neuronal transduction vectors targeting the CNS have been developed (Fu *et al.*, 2003, 2011; Puskovic *et al.*, 2004). Among the viral vectors used for gene transfer,

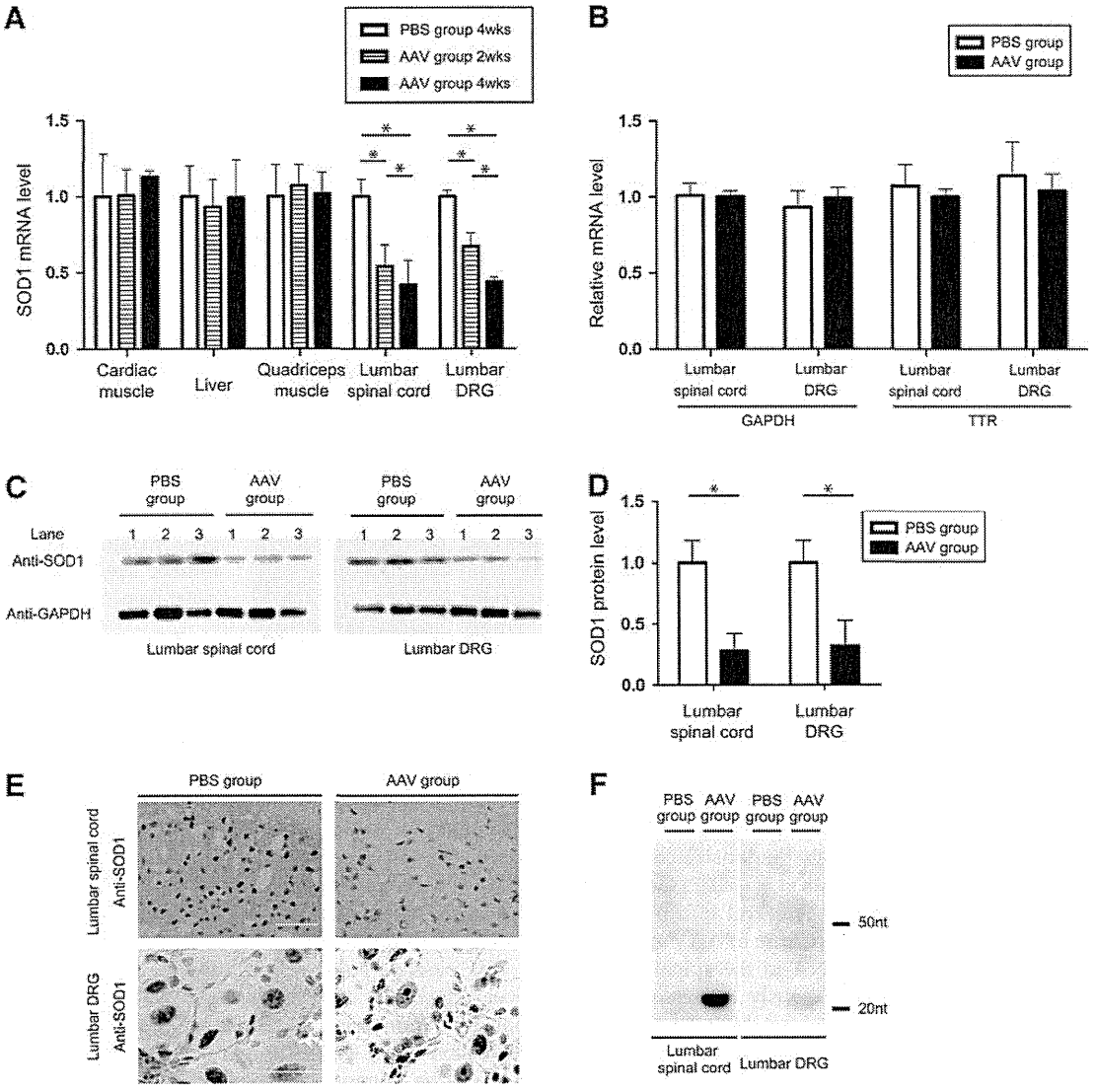

FIG. 2. Expression of *SOD1* mRNA in various tissues, reduction of SOD1 protein expression, and expression of *SOD1* shRNA in the lumbar spinal cord and DRG of mice. **(A)** Quantitative RT-PCR analysis of *SOD1* mRNA expression in cardiac muscle, liver, quadriceps muscle, lumbar spinal cord, and lumbar DRG in mice 2 and 4 weeks after injection of PBS (control) or the shRNA-AAV9 vector. *SOD1* mRNA expression was significantly ($*p<0.05$) inhibited in the lumbar spinal cord and DRG of the AAV-treated group 2 weeks after injection. In addition, expression was reduced in a time-dependent manner. Data are presented as means ± 1 SD ($n=4$ or 5 mice per group). **(B)** Quantitative RT-PCR analysis of endogenous mRNAs (of *TTR* and *GAPDH*) in the lumbar spinal cord and DRG (removed 4 weeks after injection) relative to total input RNA. Data are presented as means ± 1 SD ($n=4$ or 5 mice per group; $*p<0.05$). **(C** and **D)** SOD1 protein levels of three mice, as assessed by Western blot analysis 4 weeks after injection of PBS or shRNA-AAV9. Data are presented as means ± 1 SD ($n=3$ mice per group; $*p<0.05$). **(E)** Expression of SOD1 based on immunohistochemical analysis in the lumbar spinal cord and lumbar DRG. **(F)** Northern blotting analysis of total RNA derived from the lumbar spinal cord and DRG, 4 weeks after injection of PBS or shRNA AAV9. The 21-nucleotide antisense bands indicative of functional siRNA were detected. DRG, dorsal root ganglia; GAPDH, glyceraldehyde-3-phosphate dehydrogenase; SOD1, superoxide dismutase-1; TTR, transthyretin. Color images available online at www.liebertpub.com/hgtb

AAV vectors have the advantage of conferring stable, long-term gene expression in the absence of an inflammatory response (Kaemmerer *et al.*, 2000). Therefore, AAV vectors have been used for gene therapy targeting neurological disorders, and the different transduction abilities of various AAV vector serotypes have been investigated. The AAV9 vector has the highest infectivity for neural tissue in a rodent model (Storek *et al.*, 2008; Bevan *et al.*, 2011; Federici *et al.*, 2011). Among AAV serotypes, including AAV1, AAV6, and AAV8, intrathecal injection of an AAV9 vector encoding green fluorescent protein is the most effective for biodistribution and transduction in the spinal cord and DRG of mice (Storek *et al.*, 2008; Snyder *et al.*, 2011). We therefore chose AAV9 as the vector for gene delivery to the spinal cord and DRG and found that it stably expressed the transgene in both tissues.

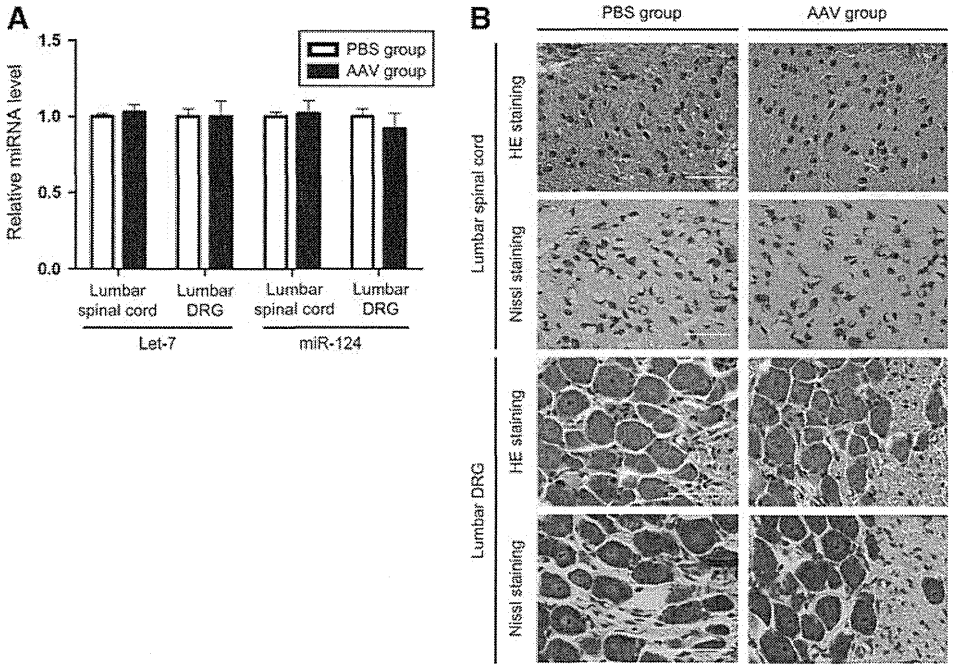

FIG. 3. Lack of change in the expression of endogenous miRNAs in the lumbar spinal cord and dorsal root ganglia (DRG), and absence of histological abnormalities in these structures, after shRNA-AAV9 injection. **(A)** Quantification of endogenous levels of the miRNAs let-7 and miR-124 in the lumbar spinal cord and DRG, determined by quantitative RT-PCR. Data are presented as means ± 1 SD ($n=3$ mice per group; $^*p<0.05$). **(B)** Hematoxylin–eosin (HE) and Nissl staining were done to demonstrate the absence of abnormalities in either the lumbar spinal cord or DRG. Scale bars: 50 μm.

We chose *SOD1* as the target gene in the spinal cord, because siRNA targeting wild-type *SOD1* halts familial amyotrophic lateral sclerosis (ALS) caused by *SOD1* mutation by silencing the mutant gene in siRNA-expressing transgenic mice, as we had previously demonstrated as proof of principle (Saito *et al.*, 2005; Yokota *et al.*, 2007). Moreover, we think that *SOD1* is an appropriate and effective endogenous gene for evaluating side effects due to AAV-associated toxicity and overexpression of shRNA in the spinal neurons and DRG, because *SOD1* is ubiquitously expressed in the CNS and because *SOD1* knockout mice exhibit no neurological phenotypes except for enhanced susceptibility to axonal injury and cerebral ischemia (Reaume *et al.*, 1996; Kawase *et al.*, 1999).

Our results demonstrated that intrathecal administration of shRNA-AAV9 reduced the mRNA expression levels of the targeted molecule by approximately 60% in both the spinal cord and the DRG, and that this reduction persisted for at least 4 weeks.

Although this reduction might not be considered robust, it may be sufficient to alter an associated phenotype in mice. Even partial reduction of SOD1 production in the spinal cord is suggested to have a substantial therapeutic effect on the ALS phenotype, because the copy number of the mutant transcript (G93A SOD1) and the severity of the ALS phenotype are closely associated in SOD1G93A transgenic mice. (Alexander *et al.*, 2004) Similarly, in the DRG, partial knockdown of transient receptor potential vanilloid-1 (TRPV1) by about 75% in shRNA-transgenic mice decreases the development of inflammatory thermal hyperalgesia after spinal nerve ligation (Christoph *et al.*, 2008). These results indicate that even modest reduction of target gene expression may be sufficient for effective gene therapy. Moreover, excess expression of shRNA, to the extent that target gene expression is nearly completely suppressed, may outcompete miRNA or pre-miRNAs and oversaturate components of the endogenous miRNA processing machinery, such as exportin-5 and Ago2, resulting in cellular damage due to miRNA deficiency (Grimm *et al.*, 2006; Rossi, 2008). In the current study, the expression of endogenous miRNAs was unchanged after administration of shRNA-AAV9, suggesting that the viral dose we used might have been sufficient for a silencing effect and might have fallen within the therapeutic window, where toxicity does not occur.

One possible strategy for "tuning" the shRNA expression level is the use of inducible promoters such as the tetracycline-inducible promoter (Kappel *et al.*, 2007). In this situation, expression of the shRNA might be "switched on" temporarily through the systemic addition of doxycycline but "switched off" (e.g., when the silencing effect is excessive or shRNA toxicity is observed) by withdrawal of doxycycline. Thus, the silencing effect on the target gene after intrathecal injection of shRNA-AAV9 might be adjusted on demand through the use of an inducible promoter for shRNA expression.

Although we confirmed that the gene-silencing effect in the spinal cord and DRG persisted for as long as 4 weeks in our mice, we did not examine persistence beyond this time point. The protein expression that is induced systemically after AAV injection has been reported to reduce target gene expression in humans for months, and this result likely reflects immunological elimination of shRNA-AAV complexes by $CD8^+$ memory T cells (Peden *et al.*, 2004; Yokota *et al.*, 2004; Manno *et al.*, 2006). However, AAV vector constructs that are injected directly into the CNS are well known to show prolonged expression of their transgenes without the induction of an immune response (Janson *et al.*, 2002; Marks *et al.*, 2008; Worgall *et al.*, 2008). In addition, we previously demonstrated that shRNA-transgenic mice that expressed the same shRNA as used in the present study showed significant suppression of *SOD1* for longer than 1 year (Saito *et al.*, 2005). Accordingly, we believe that the AAV vector we used here can stably express the transgene

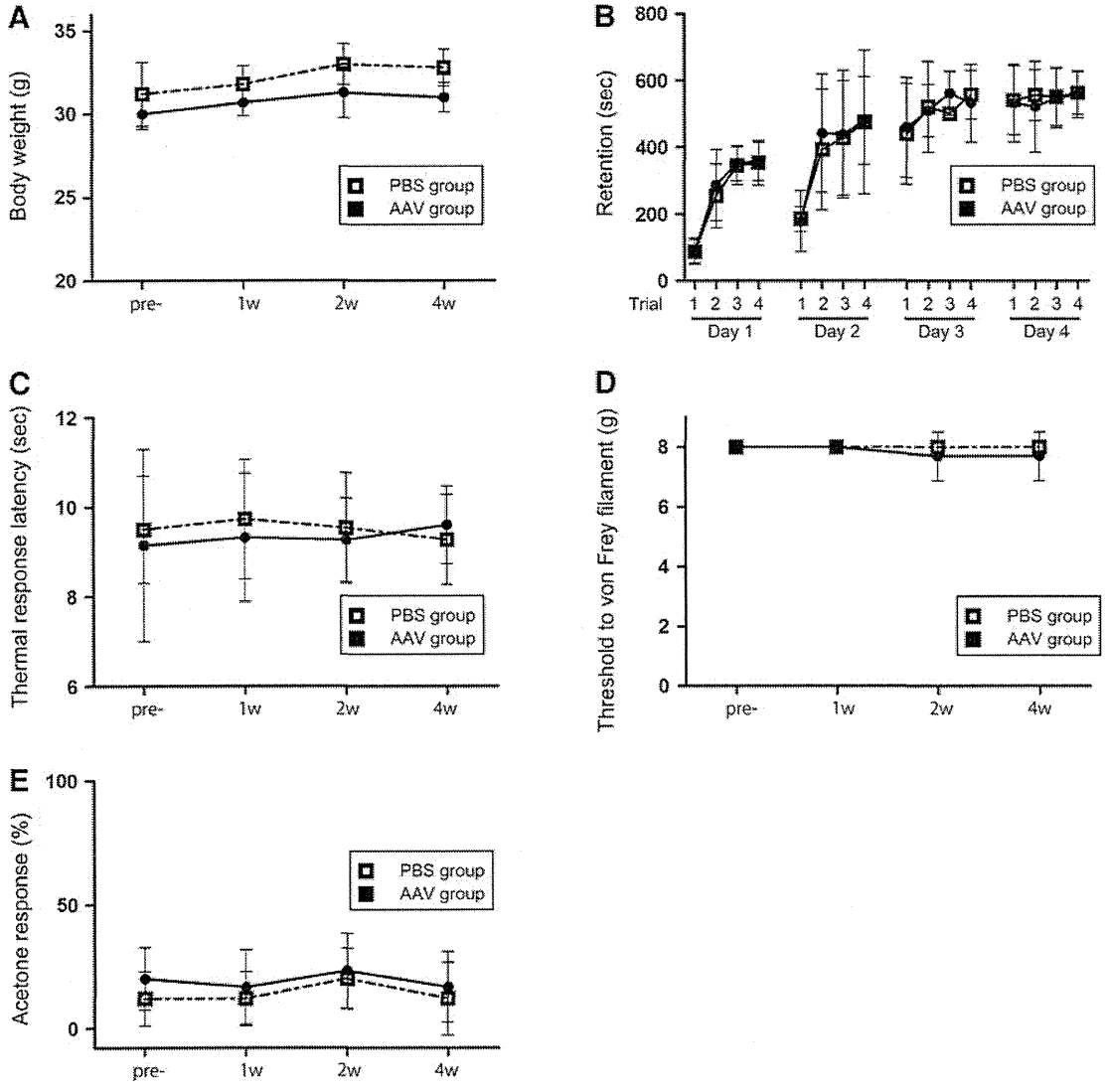

FIG. 4. Assessment of body weight, locomotion, and plantar sensation in the hind limbs of PBS- and AAV-treated mice. **(A)** Throughout the 4-week experimental period, body weight remained similar in PBS- and AAV-treated mice. Data are presented as means ± 1 SD ($n = 6$ mice per group; $p > 0.05$). **(B)** In the accelerating Rotarod test performed 4 weeks after injection, all mice in both the PBS- and AAV-treated groups demonstrated similar performance levels. Each mouse was trained in four trials daily for a total of 4 days. Data are presented as means ± 1 SD ($n = 6$ mice per group; $p > 0.05$). **(C)** Latency of response to heat stimulation, **(D)** threshold for von Frey filaments, and **(E)** response to acetone application. No significant differences were observed between the PBS- and AAV-treated groups. Data are represented as means ± 1 SD ($n = 6$ mice per group; $p > 0.05$).

and achieve long-term suppression of target gene expression in the CNS.

In general, intrathecal injection of a viral vector is a safe, minimally invasive, and sound approach (Sakura *et al.*, 1996; Pogatzki *et al.*, 2000). Using this route with AAV vector, we showed that target gene mRNA expression was not decreased in cardiac and skeletal muscles or liver. Therefore, intrathecally injected AAV9 likely remains localized within, and is specific for, the CNS. Moreover, through the use of intensive motor and sensory behavioral tests, we confirmed the lack of adverse effect associated with this method. Our study showed that intrathecal administration of an AAV9-based vector does not damage the tissues histologically or alter the expression of unrelated endogenous mRNAs in the spinal cord and DRG. Thus, we consider that intrathecal injection of shRNA-AAV9 is sufficiently safe for clinical application.

For the treatment of diseases causing intractable pain, intrathecally administered siRNA had been used to target molecules such as the δ opioid receptor (Luo *et al.*, 2005), TRPV1 (Christoph *et al.*, 2006), and the NR1 (Garraway *et al.*, 2009) and NR2B (Tan *et al.*, 2005) subunits of the *N*-methyl-D-aspartic acid receptor in the spinal cord or DRG. Similarly, the intrathecal shRNA-AAV9 approach might be used as therapy for pathological states in which central molecular integrators of nociceptive or pain-related receptors are activated, such as Sjögren's neuropathy (Pavlakis *et al.*, 2011), complex regional pain syndrome (Wei *et al.*, 2009), cancer pain (Pan *et al.*, 2010), and the hypersensitivity of sensory

neurons involved in chronic neuropathic pain (Luo *et al.*, 2005; Christoph *et al.*, 2006; Garraway *et al.*, 2009).

To our knowledge, our study is the first to demonstrate that intrathecal injection of AAV9 vector encoding shRNA is safe and effective for the suppression of target gene expression in the spinal cord and DRG of mice. Although further investigations are needed to optimize the dose and components of the vector construct, our study represents an important step in advancing the clinical use of a viral vector encoding an shRNA as a promising system for gene therapy.

Acknowledgments

The authors thank Madoka Ukegawa, M.D., Department of Orthopedic Surgery, Graduate School of Tokyo Medical and Dental University, for technical support, and Miyoko Ojima, Graduate School, Tokyo Medical and Dental University, for technical support and helpful advice. This work was done in Tokyo, Japan, and was supported in part through a Grant-in-Aid for Scientific Research from the Japan Society for the Promotion of Science and by grants from the Japan Orthopedics and Traumatology Foundation (no. 217), the National Institute of Biomedical Innovation, Japan (to T.Y.), and the Ministry of Health, Labor, and Welfare, Japan (to T.Y. [#2212070] and H.M. [#2212148]).

Author Disclosure Statement

There is no conflict of interest to disclose.

References

Alexander, G.M., Erwin, K.L., Byers, N., *et al.* (2004). Effect of transgene copy number on survival in the G93A SOD1 transgenic mouse model of ALS. Brain Res. Mol. Brain Res. 130, 7–15.

Bevan, A.K., Duque, S., Foust, K.D., *et al.* (2011). Systemic gene delivery in large species for targeting spinal cord, brain, and peripheral tissues for pediatric disorders. Mol. Ther. 19, 1971–1980.

Bish, L.T., Morine, K., Sleeper, M.M., *et al.* (2008). Adeno-associated virus (AAV) serotype 9 provides global cardiac gene transfer superior to AAV1, AAV6, AAV7, and AAV8 in the mouse and rat. Hum. Gene Ther. 19, 1359–1368.

Christoph, T., Grünweller, A., Mika, J., *et al.* (2006). Silencing of vanilloid receptor TRPV1 by RNAi reduces neuropathic and visceral pain *in vivo*. Biochem. Biophys. Res. Commun. 350, 238–243.

Christoph, T., Bahrenberg, G., De Vry, J., *et al.* (2008). Investigation of TRPV1 loss-of-function phenotypes in transgenic shRNA expressing and knockout mice. Mol. Cell. Neurosci. 37, 579–589.

Dorn, G., Patel, S., Wotherspoon, G., *et al.* (2004). siRNA relieves chronic neuropathic pain. Nucleic Acids Res. 32, e49.

Federici, T., Taub, J.S., Baum, G.R., *et al.* (2011). Robust spinal motor neuron transduction following intrathecal delivery of AAV9 in pigs. Gene Ther. 15. doi: 10.1038/gt.2011.130.

Fire, A., Xu, S., Montgomery, M.K., *et al.* (1998). Potent and specific genetic interference by double-stranded RNA in *Caenorhabditis elegans*. Nature 391, 806–811.

Fu, H., Muenzer, J., Samulski, R.J., *et al.* (2003). Self-complementary adeno-associated virus serotype 2 vector: Global distribution and broad dispersion of AAV-mediated transgene expression in mouse brain. Mol. Ther. 8, 911–917.

Fu, H., Dirosario, J., Killedar, S., *et al.* (2011). Correction of neurological disease of mucopolysaccharidosis IIIB in adult mice by rAAV9 trans-blood–brain barrier gene delivery. Mol. Ther. 19, 1025–1033.

Fu, Y., Zhang, Q., Kang, C., *et al.* (2009). Inhibitory effects of adenovirus mediated COX-2, Akt1 and PIK3R1 shRNA on the growth of malignant tumor cells *in vitro* and *in vivo*. Int. J. Oncol. 35, 583–591.

Garraway, S.M., Xu, Q., and Inturrisi, C.E. (2009). siRNA-mediated knockdown of the NR1 subunit gene of the NMDA receptor attenuates formalin-induced pain behaviors in adult rats. J. Pain 10, 380–390.

Gregorevic, P., Blankinship, M.J., Allen, J.M., *et al.* (2004). Systemic delivery of genes to striated muscles using adeno-associated viral vectors. Nat. Med. 10, 828–834.

Grimm, D., Streetz, K.L., Jopling, C.L., *et al.* (2006). Fatality in mice due to oversaturation of cellular microRNA/short hairpin RNA pathways. Nature 441, 537–541.

Hargreaves, K., Dubner, R., Brown, F., *et al.* (1988). A new and sensitive method for measuring thermal nociception in cutaneous hyperalgesia. Pain 32, 77–88.

Hassani, Z., Lemkine, G.F., Erbacher, P., *et al.* (2005). Lipid-mediated siRNA delivery down-regulates exogenous gene expression in the mouse brain at picomolar levels. J. Gene Med. 7, 198–207.

Hermens, W.T., Ter Brake, O., Dijkhuizen, P.A., *et al.* (1999). Purification of recombinant adeno-associated virus by iodixanol gradient ultracentrifugation allows rapid and reproducible preparation of vector stocks for gene transfer in the nervous system. Hum. Gene Ther. 10, 1885–1891.

Janson, C., McPhee, S., Bilaniuk, L., *et al.* (2002). Clinical protocol: Gene therapy of Canavan disease: AAV-2 vector for neurosurgical delivery of aspartoacylase gene (ASPA) to the human brain. Hum. Gene Ther. 13, 1391–1412.

Kaemmerer, W.F., Reddy, R.G., Warlick, C.A., *et al.* (2000). *In vivo* transduction of cerebellar Purkinje cells using adeno-associated virus vectors. Mol. Ther. 2, 446–457.

Kappel, S., Matthess, Y., Kaufmann, M., and Strebhardt, K. (2007). Silencing of mammalian genes by tetracycline-inducible shRNA expression. Nat. Protoc. 2, 3257–3269.

Kawase, M., Murakami, K., Fujimura, M., *et al.* (1999). Exacerbation of delayed cell injury after transient global ischemia in mutant mice with CuZn superoxide dismutase deficiency. Stroke 30, 1962–1968.

Li, G., Li, D., Xie, Q., *et al.* (2008). RNA interfering connective tissue growth factor prevents rat hepatic stellate cell activation and extracellular matrix production. J. Gene Med. 10, 1039–1047.

Luo, M.C., Zhang, D.Q., Ma, S.W., *et al.* (2005). An efficient intrathecal delivery of small interfering RNA to the spinal cord and peripheral neurons. Mol. Pain 1, 29.

Manno, C.S., Pierce, G.F., Arruda, V.R., *et al.* (2006). Successful transduction of liver in hemophilia by AAV-Factor IX and limitations imposed by the host immune response. Nat. Med. 12, 342–347.

Marks, W.J., Ostrem, J.L., Verhagen, L., *et al.* (2008). Safety and tolerability of intraputaminal delivery of CERE-120 (adeno-associated virus serotype 2-neurturin) to patients with idiopathic Parkinson's disease: An open-label, phase I trial. Lancet Neurol. 7, 400–408.

Mayra, A., Tomimitsu, H., Kubodera, T., *et al.* (2011). Intraperitoneal AAV9-shRNA inhibits target expression in neonatal skeletal and cardiac muscles. Biochem. Biophys. Res. Commun. 405, 204–209.

Mikami, M., and Yang, J. (2005). Short hairpin RNA-mediated selective knockdown of NaV1.8 tetrodotoxin-resistant voltage-gated sodium channel in dorsal root ganglion neurons. Anesthesiology 103, 828–836.

Mitchell, M., Jerebtsova, M., Batshaw, M.L., *et al.* (2000). Long-term gene transfer to mouse fetuses with recombinant adenovirus and adeno-associated virus (AAV) vectors. Gene Ther. 7, 1986–1992.

Pan, H.L., Zhang, Y.Q., and Zhao, Z.Q. (2010). Involvement of lysophosphatidic acid in bone cancer pain by potentiation of TRPV1 via PKCε pathway in dorsal root ganglion neurons. Mol. Pain 6, 85.

Pavlakis, P.P., Alexopoulos, H., Kosmidis, M.L., *et al.* (2011). Peripheral neuropathies in Sjögren syndrome: A new reappraisal. J. Neurol. Neurosurg. Psychiatry 82, 798–802.

Peden, C.S., Burger, C., Muzyczka, N., and Mandel, R.J. (2004). Circulating anti-wild-type adeno-associated virus type 2 (AAV2) antibodies inhibit recombinant AAV2 (rAAV2)-mediated, but not rAAV5-mediated, gene transfer in the brain. J. Virol. 78, 6344–6359.

Pogatzki, E.M., Zahn, P.K., and Brennan, T.J. (2000). Lumbar catheterization of the subarachnoid space with a 32-gauge polyurethane catheter in the rat. Eur. J. Pain 4, 111–113.

Puskovic, V., Wolfe, D., Goss, J., *et al.* (2004). Prolonged biologically active transgene expression driven by HSV LAP2 in brain *in vivo*. Mol. Ther. 10, 67–75.

Reaume, A.G., Elliott, J.L., Hoffman, E.K., *et al.* (1996). Motor neurons in Cu/Zn superoxide dismutase-deficient mice develop normally but exhibit enhanced cell death after axonal injury. Nat. Genet. 13, 43–47.

Rodriguez-Lebron, E., Denovan-Wright, E.M., Nash, K., *et al.* (2005). Intrastriatal rAAV-mediated delivery of anti-huntingtin shRNAs induces partial reversal of disease progression in R6/1 Huntington's disease transgenic mice. Mol. Ther. 12, 618–633.

Rossi, J.J. (2008). Expression strategies for short hairpin RNA interference triggers. Hum. Gene Ther. 19, 313–317.

Saito, Y., Yokota, T., Mitani, T., *et al.* (2005). Transgenic small interfering RNA halts amyotrophic lateral sclerosis in a mouse model. J. Biol. Chem. 280, 42826–42830.

Sakura, S., Hashimoto, K., Bollen, A.W., *et al.* (1996). Intrathecal catheterization in the rat: Improved technique for morphologic analysis of drug-induced injury. Anesthesiology 85, 1184–1189.

Senechal, Y., Kelly, P.H., Cryan, J.F., *et al.* (2007). Amyloid precursor protein knockdown by siRNA impairs spontaneous alternation in adult mice. J. Neurochem. 102, 1928–1940.

Senn, C., Hangartner, C., Moes, S., *et al.* (2005). Central administration of small interfering RNAs in rats: A comparison with antisense oligonucleotides. Eur. J. Pharmacol. 522, 30–37.

Snyder, B.R., Gray, S.J., Quach, E.T., *et al.* (2011). Comparison of adeno-associated viral vector serotypes for spinal cord and motor neuron gene delivery. Hum. Gene Ther. 22, 1129–1135.

Storek, B., Reinhardt, M., Wang, C., *et al.* (2008). Sensory neuron targeting by self-complementary AAV8 via lumbar puncture for chronic pain. Proc. Natl. Acad. Sci. U.S.A. 105, 1055–1060.

Tan, P.H., Yang, L.C., Shih, H.C., *et al.* (2005). Gene knockdown with intrathecal siRNA of NMDA receptor NR2B subunit reduces formalin-induced nociception in the rat. Gene Ther. 12, 59–66.

Towne, C., Raoul, C., Schneider, B.L., and Aebischer, P. (2008). Systemic AAV6 delivery mediating RNA interference against SOD1: Neuromuscular transduction does not alter disease progression in fALS mice. Mol. Ther. 16, 1018–1025.

Uno, Y., Piao, W., Miyata, K., *et al.* (2011). High-density lipoprotein facilitates *in vivo* delivery of α-tocopherol-conjugated short-interfering RNA to the brain. Hum. Gene Ther. 22, 711–719.

Wei, T., Li, W.W., Guo, T.Z., *et al.* (2009). Post-junctional facilitation of substance P signaling in a tibia fracture rat model of complex regional pain syndrome type I. Pain 144, 278–286.

Worgall, S., Sondhi, D., Hackett, N.R., *et al.* (2008). Treatment of late infantile neuronal ceroid lipofuscinosis by CNS administration of a serotype 2 adeno-associated virus expressing CLN2 cDNA. Hum. Gene Ther. 19, 463–474.

Yokota, T., Miyagishi, M., Hino, T., *et al.* (2004). siRNA-based inhibition specific for mutant SOD1 with single nucleotide alternation in familial ALS, compared with ribozyme and DNA enzyme. Biochem. Biophys. Res. Commun. 314, 283–291.

Yokota, T., Sasaguri, H., Saito, Y., *et al.* (2007). Increase of disease duration of amyotrophic lateral sclerosis in a mouse model by transgenic small interfering RNA. Arch. Neurol. 64, 145–146.

Address correspondence to:
Dr. Takanori Yokota
Department of Neurology and Neurological Science
Graduate School, Tokyo Medical and Dental University
1-5-45, Yushima, Bunkyo-ku
Tokyo 113-8519
Japan

E-mail: tak-yokota.nuro@tmd.ac.jp

Received for publication February 11, 2012;
accepted after revision April 5, 2012.

Published online: April 6, 2012.

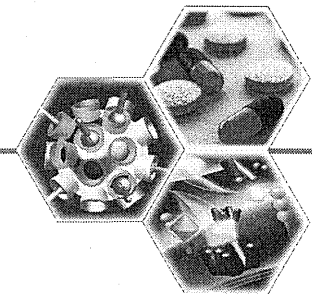

Delivery of siRNA into the blood–brain barrier: recent advances and future perspective

"Practically speaking, it may be easier to establish techniques to deliver siRNA into the blood–brain barrier rather than across it..."

Keywords: blood–brain barrier ■ brain capillary endothelial cell ■ neurological disease ■ siRNA delivery

The development of gene-silencing therapy for neurological diseases has placed great importance on the delivery of siRNA from the blood into the brain across the blood–brain barrier (BBB). Increasingly, gene-silencing therapy in the BBB itself is being considered because the BBB is associated with the pathophysiologies of many major diseases such as brain ischemia, multiple sclerosis and neurodegenerative disorders. Practically speaking, it may be easier to establish techniques to deliver siRNA into the BBB rather than across it, because there has been an accumulation of knowledge concerning the dynamic interactions between the blood circulation and brain capillary endothelial cells (BCECs), the chief components of the BBB. The purpose of this Editorial is to explain the recent advances in siRNA delivery into the BBB and to express some opinions on future research in this field.

The blood–brain barrier

The BBB is composed mainly of BCECs and has pericytes, astrocyte foot processes and nerve endings terminating at the capillary surfaces [1]. The BBB is a unique structure in the CNS that is both a physical barrier, resulting from the presence of endothelial tight junctions, and a transport barrier, resulting from selective membrane transporters and vesicular trafficking via BCECs [2]. It is generally considered that for compounds to cross the BBB they should have a molecular weight of less than 400 Da and be lipophilic [1].

The establishment of a technique to deliver siRNA across the BBB is expected to result in the development of gene-silencing therapies for a variety of neurological diseases; however, delivering siRNA across the BBB remains a challenge since siRNA molecules weigh more than 10,000 Da and are not lipophilic. So far, many technical developments have been reported such as the chemical modification of liposomal complexes with siRNA, the direct conjugation of siRNA to ligands for the BBB and the use of cell-penetrating peptides that can be noncovalently complexed or covalently linked to siRNA [3]. The precise mechanisms of these delivery strategies remain to be elucidated; therefore, most preclinical and clinical studies on the delivery of siRNA into the central nervous system have used the invasive techniques of intracerebral, intracerebroventricular or intrathecal injection into or near the targeted tissues [3]. To our knowledge, no trials have used intravascular injections to deliver siRNA across the BBB.

Pathophysiologies at the BBB

It is noteworthy that some major neurological diseases have pathophysiologies at the BBB itself, especially at BCECs, apart from those at neurons or glia [4,5]. BCECs express a range of molecules that can be targeted for silencing.

Inflammatory cell-adhesion molecules such as ICAM-1, VCAM-1, and the selectins are responsible for secondary neuronal injury after reperfusion in brain ischemia [6]. The matrix-degrading metalloproteinases (MMPs), particularly MMP-9, are involved in the process of neuroinflammation associated with the ischemic condition [7]. In an *in vitro* BBB model, silencing of MMP-9 by siRNA was reported to enhance BBB integrity [8].

Inflammatory cell-adhesion molecules are also related to the pathophysiologies of multiple sclerosis [9]. They help activated leukocytes cross the BBB and enter the brain, resulting in the initiation of immune-mediated demyelination [9]. The therapeutic concept of inhibiting

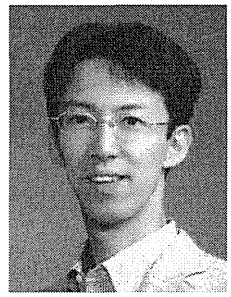

Hiroya Kuwahara
Department of Neurology & Neurological Science, Graduate School, Tokyo Medical & Dental University

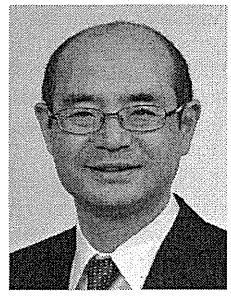

Takanori Yokota
Author of correspondence:
Department of Neurology & Neurological Science, Graduate School, Tokyo Medical & Dental University, 1–5–45, Yushima, Bunkyo-ku, Tokyo 113–8519, Japan
Tel.: +81 3 5803 5234
Fax: +81 3 5803 0169
E-mail: tak-yokota.nuro@tmd.ac.jp

Author affiliations continue overleaf...

FUTURE SCIENCE part of fsg

Hidehiro Mizusawa
Department of Neurology & Neurological Science, Graduate School, Tokyo Medical & Dental University

the adhesion of leukocytes to BCECs in multiple sclerosis is currently being employed in the clinical setting; natalizumab, a monoclonal antibody against very late antigen-4 in leukocytes, inhibits leukocytes from binding to VCAM-1 (the receptor of very late antigen-4) in BCECs [10].

In Alzheimer's disease, the receptor for advanced glycation endproducts (RAGE) in BCECs mediates the transport of the neurotoxic amyloid-β peptide from the blood into the brain, leading to oxidative stress and neuroinflammation [11]. Expression of RAGE in BCECs is approximately 2.5-times higher in Alzheimer's disease patients than in age-matched controls, and inhibition of RAGE in BCECs may alleviate the disease pathology [12].

The diseases mentioned above have a high prevalence in most developed countries, and effective therapies remain to be established. As clinicians in neurology, we wish to emphasize that the BBB itself possesses great potential as an important target for gene-silencing therapy for these diseases.

Delivery of siRNA into the BBB

Few attempts of using the concept of gene-silencing at the BBB itself have been reported. We first reported the delivery of siRNA into BCECs via a hydrodynamic injection technique [13], and the same strategy was adopted in subsequent studies [14,15]. One possible delivery mechanism of this technique is that rapid loading of an extremely large volume of solution results in a considerable increase in hydrostatic pressure in the brain capillaries. Another possible explanation is that rapid injection of a large volume of solution prevents the solution from mixing with the serum containing RNase, thereby keeping the concentration of siRNA high in the brain capillaries. However, hydrodynamic injection cannot be used clinically because it can result in injury to various organs and tissues. There is, therefore, a need to develop an alternative strategy that is clinically feasible.

We recently reported the efficient delivery of siRNA into BCECs along with endogenous lipoprotein [16]. A cholesterol-conjugated siRNA was incorporated into extracted endogenous high-density lipoproteins and then intravenously injected into mice. Cholesterol-conjugated siRNA was not delivered into neurons or glia, but was successfully delivered into BCECs by receptor-mediated uptake. Because cholesterol is taken up into BCECs along with lipoproteins but generally does not pass through the BBB, cholesterol conjugation might be an effective strategy to deliver siRNA into BCECs. To date, our report is the only one to have demonstrated a technique that enables siRNA to be delivered into BCECs and be used in a clinical setting, although improvements would need to be made before this could be done [16].

Future perspective

The biggest challenge for the efficient delivery of siRNA into BCECs is the enhancement of delivery through the reduction of tropism to the liver, secretion from the kidney and uptake into the reticuloendothelial system, such as the spleen, lymph node and bone marrow. In addition to optimizing the size, charge and lipophilicity of siRNA vectors, other possible improvements include modification of their surfaces, for example, by binding them to ligands that interact with the BCEC membrane proteins, or by coating them with polyethylene glycol to increase retention in the blood. Recently, Chen *et al.* succeeded in delivering an increased amount of a gene to BCECs by inserting polypeptides, selected from a phage library by *in vivo* panning, into the binding site of an adeno-associated virus vector to its receptor [17]. Increase in affinity to BCECs and decrease in distribution to other organs/tissues will be helpful in reducing the dosage and side effects of siRNA.

It is also important to investigate the therapeutic utility by using model animals for the neurological diseases mentioned above. Our previous reports regarding a hydrodynamic injection technique [13] and a lipoprotein vector [16] demonstrate only the proof-of-principle of siRNA delivery into BCECs by targeting organic anion transporter 3, which is exclusively expressed in BCECs in the brain and is not recognized as a pathological molecule in any neurological disease. If gene-silencing therapy in BCECs is actually demonstrated to be effective by *in vivo* delivery of siRNA in some disease models, research in this field is expected to be remarkably facilitated.

We believe that techniques to deliver siRNA into BCECs could be further developed into techniques to deliver siRNA into the brain across the BBB. Theoretically, delivery across the BBB can be achieved by using either the intercellular or intracellular route. At the BBB, there is a unique intercellular junctional complex without fenestrations that is formed from tight junctions, adherence junctions and basement membranes. Intercellular delivery across the BBB would

probably be accompanied by disruption of this junctional complex, leading to nonspecific entry of serum proteins and agents into the brain and subsequent toxicity for neurons and glia; this toxicity should be avoided.

Intracellular delivery across the BBB could result from the establishment of a method to deliver molecules into BCECs. Knowledge of the physiological transport mechanisms present at the BBB has increased remarkably [2]. A wide variety of transporters contribute to the selective influx into the brain of energy resources, amino acids, hormones and organic ions [2]. For example, glucose transporter-1, which is abundantly expressed in BCECs [18], contributes to the transport of D-glucose and vitamin C, and may work as a carrier of siRNA. Similarly, it might be possible to use amino acid transporters, monocarboxylic acid transporters or thyroid hormone transporters. However, there may be strict limitations on the structure of substrates, and it could therefore be difficult for siRNA to enter the brain via these transporters.

The unique endocytosis/transcytosis at the BBB involves a receptor-mediated mechanism (cargo such as transferrin, insulin and lipoprotein) and an adsorptive-mediated mechanism (cargo such as cationic proteins and cell-penetrating peptides) [2]. Utilization of these endocytosis/transcytosis systems may be an alternative strategy for the effective and safe delivery of macromolecules such as siRNA [19]. Short peptides derived from the rabies virus glycoprotein, which bind to the acetylcholine receptor, have been used to deliver siRNA across the BBB [20]. Other candidate ligands that can be used include the low-density lipoprotein receptor (LDLR)-binding domain of apolipoprotein B (the ligand for LDLR) [21], Angiopep-2 (the ligand for LDLR-related protein-1) [22] or the nontoxic form of the diphtheria toxin receptor, CRM197 (the ligand for diphtheria toxin receptor) [23]. To achieve delivery across the BBB, it will be necessary for the cargo to stay in the endosome during intracellular trafficking. Even if the cargo can reach the abluminal membrane of BCECs, there remain at least two hurdles to overcome: the mechanism of detaching the cargo from the BCECs and the passage through the basement membrane. Accumulating knowledge of the biology of the BBB is expected to be helpful in the establishment of a method of delivering siRNA across the BBB.

In conclusion, the pursuit of delivering siRNA into the BBB to develop gene-silencing therapy for diseases involving BCECs is noteworthy. Research from this perspective might result in important knowledge for the development of techniques to deliver siRNA from the blood into the brain across the BBB.

Financial & competing interests disclosure

This work was supported by grants from the Ministry of Health, Labour and Welfare of Japan (#2212070 and #2212148) and a grant from the Ministry of Education, Science and Culture of Japan (#20659138). The authors have no other relevant affiliations or financial involvement with any organization or entity with a financial interest in or financial conflict with the subject matter or materials discussed in the manuscript apart from those disclosed.

No writing assistance was utilized in the production of this manuscript.

References

1 Pardridge WM. Blood–brain barrier genomics. *Stroke* 38(2), 686–690 (2007).

2 Abbott NJ, Patabendige AA, Dolman DE, Yusof SR, Begley DJ. Structure and function of the blood–brain barrier. *Neurobiol. Dis.* 37(1), 13–25 (2010).

3 Mathupala SP. Delivery of small-interfering RNA (siRNA) to the brain. *Expert Opin. Ther. Pat.* 19(2), 137–140 (2009).

4 Zlokovic BV. The blood–brain barrier in health and chronic neurodegenerative disorders. *Neuron* 57(2), 178–201 (2008).

5 Neuwelt EA, Bauer B, Fahlke C *et al.* Engaging neuroscience to advance translational research in brain barrier biology. *Nat. Rev. Neurosci.* 12(3), 169–182 (2011).

6 Frijns CJ, Kappelle LJ. Inflammatory cell adhesion molecules in ischemic cerebrovascular disease. *Stroke* 33(8), 2115–2122 (2002).

7 Jin R, Yang G, Li G. Molecular insights and therapeutic targets for blood–brain barrier disruption in ischemic stroke: critical role of matrix metalloproteinases and tissue-type plasminogen activator. *Neurobiol. Dis.* 38(3), 376–385 (2010).

8 Bonoiu A, Mahajan SD, Ye L *et al.* MMP-9 gene silencing by a quantum dot-siRNA nanoplex delivery to maintain the integrity of the blood brain barrier. *Brain Res.* 1282, 142–155 (2009).

9 Simka M. Blood–brain barrier compromise with endothelial inflammation may lead to autoimmune loss of myelin during multiple sclerosis. *Curr. Neurovasc. Res.* 6(2), 132–139 (2009).

10 Ransohoff RM. Natalizumab for multiple sclerosis. *N. Engl. J. Med.* 356(25), 2622–2629 (2007).

11 Yan SD, Chen X, Fu J *et al.* RAGE and amyloid-β peptide neurotoxicity in Alzheimer's disease. *Nature* 382(6593), 685–691 (1996).

12 Deane R, Yan SD, Submamaryan RK *et al.* RAGE mediates amyloid-β peptide transport across the blood–brain barrier and accumulation in brain. *Nat. Med.* 9(7), 907–913 (2003).

13 Hino T, Yokota T, Ito S *et al. In vivo* delivery of small interfering RNA targeting brain capillary endothelial cells. *Biochem. Biophys. Res. Commun.* 340(1), 263–267 (2006).

14 Campbell M, Kiang AS, Kenna PF *et al.* RNAi-mediated reversible opening of the blood–brain barrier. *J. Gene. Med.* 10(8), 930–947 (2008).

15 Fuest C, Bankstahl M, Winter P, Helm M, Pekcec A, Potschka H. *In vivo* down-regulation of mouse brain capillary P-glycoprotein: a preliminary investigation. *Neurosci. Lett.* 464(1), 47–51 (2009).

16 Kuwahara H, Nishina K, Yoshida K *et al.* Efficient *in vivo* delivery of siRNA into brain capillary endothelial cells along with endogenous lipoprotein. *Mol. Ther.* 19(12), 2213–2221 (2011).

17 Chen YH, Chang M, Davidson BL. Molecular signatures of disease brain endothelia provide new sites for CNS-directed enzyme therapy. *Nat. Med.* 15(10), 1215–1218 (2009).

18 Uchida Y, Ohtsuki S, Katsukura Y *et al.* Quantitative targeted absolute proteomics of human blood–brain barrier transporters and receptors. *J. Neurochem.* 117(2), 333–345 (2011).

19 Lichota J, Skjørringe T, Thomsen LB, Moos T. Macromolecular drug transport into the brain using targeted therapy. *J. Neurochem.* 113(1), 1–13 (2010).

20 Kumar P, Wu H, McBride JL *et al.* Transvascular delivery of small interfering RNA to the central nervous system. *Nature* 448(7149), 39–43 (2007).

21 Spencer BJ, Verma IM. Targeted delivery of proteins across the blood–brain barrier. *Proc. Natl Acad. Sci. USA.* 104(18), 7594–7599 (2007).

22 Demeule M, Currie JC, Bertrand Y *et al.* Involvement of the low-density lipoprotein receptor-related protein in the transcytosis of the brain delivery vector angiopep-2. *J. Neurochem.* 106(4), 1534–1544 (2008).

23 Gaillard PJ, de Boer AG. 2B-trans technology: targeted drug delivery across the blood–brain barrier. *Methods Mol. Biol.* 437, 161–175 (2008).

Biomaterials 33 (2012) 2770–2779

Contents lists available at SciVerse ScienceDirect

Biomaterials

journal homepage: www.elsevier.com/locate/biomaterials

Enhanced stability and gene silencing ability of siRNA-loaded polyion complexes formulated from polyaspartamide derivatives with a repetitive array of amino groups in the side chain

Tomoya Suma [a], Kanjiro Miyata [b], Takehiko Ishii [a], Satoshi Uchida [b], Hirokuni Uchida [a], Keiji Itaka [b], Nobuhiro Nishiyama [b], Kazunori Kataoka [a,b,c,d,*]

[a] Department of Bioengineering, Graduate School of Engineering, The University of Tokyo, 7-3-1 Hongo, Bunkyo-ku, Tokyo 113-8656, Japan
[b] Center for Disease Biology and Integrative Medicine, Graduate School of Medicine, The University of Tokyo, 7-3-1 Hongo, Bunkyo-ku, Tokyo 113-0033, Japan
[c] Department of Materials Engineering, Graduate School of Engineering, The University of Tokyo, 7-3-1 Hongo, Bunkyo-ku, Tokyo 113-8656, Japan
[d] Center for NanoBio Integration, The University of Tokyo, 7-3-1 Hongo, Bunkyo-ku, Tokyo 113-8656, Japan

ARTICLE INFO

Article history:
Received 12 October 2011
Accepted 9 December 2011
Available online 24 December 2011

Keywords:
siRNA
Poly(amino acid)
Polyion complex
Charge density
Endosomal escape

ABSTRACT

The delivery of siRNA therapeutics owes its success to the development of carrier systems with high efficacy and minimum toxicity. Here, cationic polyaspartamide derivatives with a regulated number and spacing of positively charged amino groups in the side chain were prepared from a single platform polymer of poly(β-benzyl L-aspartate) to assess their availability as siRNA carriers through polyion complex (PIC) formation. These polymers have 1,2-diaminoethane, 1,3-diaminopropane, and *N,N'*-bis(2-aminoethyl)-1,2-diaminoethane moieties in the side chain, and are termed as PAsp(DET), PAsp(DPT), and PAsp(TEP), respectively. siRNA-loaded PICs stable in serum-containing media were formed from PAsp(TEP) and PAsp(DPT) with two positive charges in the side chain at pH 7.4, whereas no such stable PIC was obtained from PAsp(DET) with only a single charge in the side chain, suggesting facilitated multivalent interactions with siRNA molecules to increase the PIC stability. The PAsp(DPT) and PAsp(TEP) PICs stable in the serum-containing media underwent an appreciably enhanced uptake into cultured cells through endocytosis, and subsequently exerted effective endosomal escape for the significant silencing of target gene expression. Notably, PAsp(TEP) PIC displayed negligible cytotoxicity in sharp contrast to the highly toxic feature of PAsp(DPT) PIC. This cytotoxicity is apparently correlated with the minimal damage to the cytoplasmic membrane of cells exposed to PAsp(TEP) at pH 7.4 evidenced from the fluorescent dye (YO-PRO-1) permeation assay. There was, in turn, a significant increase in YO-PRO-1 permeability at endosomal pH of 5.5 for PAsp(TEP)-exposed cells, indicating that PAsp(TEP) exerts membrane damage in a pH-selective manner, and eventually facilitates the translocation of siRNA-loaded PIC from the acidic endosomal compartment into the cytoplasm for effective gene silencing without any severe toxicity at physiological conditions. This acidic pH modulated enhancement in membrane damage of PAsp(TEP) may be explained by an increased protonation of the arrayed amino groups in the side chain that strongly perturb the endosomal membrane integrity. Eventually, PAsp(TEP) with a side chain array of pH-sensitive amino groups was demonstrated to be a promising component for constructing siRNA carriers exerting effective gene silencing in a less toxic context.

1. Introduction

Small interfering RNA (siRNA) enables the target-specific gene silencing through RNA interference (RNAi) machinery and has been intensely desired as a pharmaceutical agent for the treatment of various intractable diseases, such as cancers, viral infections, and genetic disorders [1]. However, siRNA has the inherent problem of poor bioavailability, such as the rapid decomposition in the body and inefficient cellular internalization. Thus, development of safe and effective delivery systems for siRNA is a current challenge for siRNA-based therapies.

Polyion complexes (PICs) formed from electrostatic interaction of polycations and anionic oligonucleotides, including siRNA, can protect oligonucleotides from enzymatic degradation and facilitate

* Corresponding author. Department of Materials Engineering, Graduate School of Engineering, The University of Tokyo, 7-3-1 Hongo, Bunkyo-ku, Tokyo 113-8656, Japan. Tel.: +81 35841 7138; fax: +81 3 5841 7139.
E-mail address: kataoka@bmw.t.u-tokyo.ac.jp (K. Kataoka).

0142-9612/$ – see front matter © 2011 Elsevier Ltd. All rights reserved.
doi:10.1016/j.biomaterials.2011.12.022

their cellular uptake. These PICs present a promising candidate for oligonucleotide carriers [2–5]. The most widely studied polycations in this regard are polyethylenimine (PEI) and its derivatives, which have low pKa amino groups contributing to a facilitated endosomal escape of PICs through the so-called proton sponge effect [6,7]. Although several studies have demonstrated significant gene silencing with siRNA-loaded PICs prepared from PEI derivatives [8–10], their cytotoxic effect is frequently a concern for clinical applications [11–13]. Accordingly, polycations showing highly efficient endosomal escape and minimal cytotoxicity in clinical settings are required for the practical formulation of siRNA-loaded PICs.

In the previous study, we reported that a polyaspartamide derivative bearing a 1,2-diaminoethane unit in the side chain (PAsp(DET)) (Fig. 1) exerted efficient and low toxic translocation of its PIC with plasmid DNA (pDNA) from the endosomal compartment into the cytoplasm through pH-selective membrane disruption [14–16]. The 1,2-diaminoethane unit in the side chain of PAsp(DET) changed from a mono-protonated state to di-protonated state responding to the pH drop in the endosomal compartment, which facilitated the interaction of PAsp(DET) with the endosomal membrane. Eventually, pDNA/PAsp(DET) PIC achieved appreciable *in vivo* transfection efficiency to show a therapeutic outcome in diseased animal models [17–20]. Nevertheless, the use of PAsp(DET) in siRNA transfection resulted in no significant efficacy because of the poor stability of siRNA/PAsp(DET) PIC in serum-containing media [21,22], suggesting that the substantially decreased number of anionic charges of siRNA compared to pDNA might reduce the association force in PIC formation with PAsp(DET). Here, we report that this stability issue of siRNA-loaded PIC was overcome by constructing a repetitive array of aminoethylene units in the side chain of the polycation to exert multivalent electrostatic interactions with siRNA, retaining both endosomal escaping functions and tolerability in serum-containing medium. Furthermore, by tuning the spacer length between repeating amine units, the toxicity issue can also be managed to construct the siRNA-loaded PIC with well-balanced properties of highly specific gene silencing potential and appreciably low cytotoxicity.

2. Materials and methods

2.1. Materials

β-Benzyl L-aspartate *N*-carboxy anhydride (BLA-NCA) was purchased from Chuo Kaseihin Co., Inc. (Tokyo, Japan). *N,N*-Dimethylformamide (DMF), dichloromethane (DCM), *n*-butylamine, diethylenetriamine (DET), tetraethylenepenatamine (TEP), dipropylenetriamine (DPT), and *N*-methyl-2-pyrrolidone (NMP) were purchased from Wako Pure Chemical Industries, Ltd. (Osaka, Japan). DMF, DCM, NMP, *n*-butylamine, DET, TEP, and DPT were distilled before use. A luciferase-expressing mouse melanoma cell line, B16F10-Luc, was purchased from Caliper LifeScience (Hopkinton, MA). Dulbecco's modified eagle's medium (DMEM) was purchased from Sigma–Aldrich Co. (St. Louis, MO). Fetal bovine serum (FBS) was purchased from Dainippon Sumitomo Pharma Co, Ltd. (Osaka, Japan). ExGen 500 was purchased from Fermentas (Ontario, Canada). Luciferase Assay System was purchased from Promega Co. (Madison, WI). All the siRNA molecules including 5′-Cy3-labeled siRNAs were synthesized by Hokkaido System Science (Hokkaido, Japan). The sequences are as follows: firefly luciferase siRNA (sense: 5′-(Cy3-) CUU ACG CUG AGU ACU UCG AdTdT-3′, antisense: 5′-UCG AAG UAC UCA GCG UAA GdTdT-3′) and scrambled siRNA (sense: 5′-UUC UCC GAA CGU GUC ACG UdTdT-3′, antisense: 5′-ACG UGA CAC GUU CGG AGA AdTdT-3′).

2.2. Synthesis of poly(β-benzyl L-aspartate) (PBLA)

PBLA was synthesized by the ring-opening polymerization of BLA-NCA initiated by *n*-butylamine as previously reported [23]. Briefly, *n*-butylamine (6 μL, 0.06 mmol) in DCM (490 μL) was added to BLA-NCA (1.40 g, 4.86 mmol) dissolved in 16.4 mL of DCM/DMF (9:1 v/v). The reaction solution was stirred for 48 h at 35 °C under an argon atmosphere. The solution was precipitated in hexane/ethyl acetate (6:4 v/v) and dried under reduced pressure overnight to obtain PBLA (888 mg, yield 77%). Size exclusion chromatography (SEC) was performed to determine the molecular weight distribution (MWD) of the obtained PBLA using a TOSOH HLC-8220 equipped with TSK gel columns (SuperAW4000 and SuperAW3000 × 2, TOSHO, Japan) and an internal refractive index (RI) detector at a flow rate of 0.3 mL min^{-1} at 40 °C. NMP with 10 mL LiBr was used as an eluent. A narrow MWD (Mw/Mn = 1.02) was confirmed from the SEC (data not shown). The degree of polymerization (DP) of the PBLA was calculated to be 92 from the peak intensity ratio of the butyl protons ($CH_3CH_2CH_2CH_2$-, δ = 0.8–1.5 ppm) at the α-chain end to the benzyl protons ($C_6H_5CH_2$-, δ = 5.1 and 7.3 ppm) at the side chain in the ^{1}H NMR spectrum (concentration: 10 mg/mL, solvent: dimethyl sulfoxide-d_6, temperature: 80 °C) (data not shown).

2.3. Synthesis of a series of cationic polyaspartamide derivatives, poly{N-[N′-(2-aminoethyl)-2-aminoethyl]aspartamide} (PAsp(DET)), poly{N-(N′-{N″-[N‴-(2-aminoethyl)-2-aminoethyl]-2-aminoethyl}-2-aminoethyl)aspartamide} (PAsp(TEP)), and poly{N-[N′-(3-aminopropyl)-3-aminopropyl]aspartamide} (PAsp(DPT))

PAsp(DET), PAsp(TEP), and PAsp(DPT) were prepared through the aminolysis reaction of PBLA with DET, TEP, and DPT, respectively, according to the previously

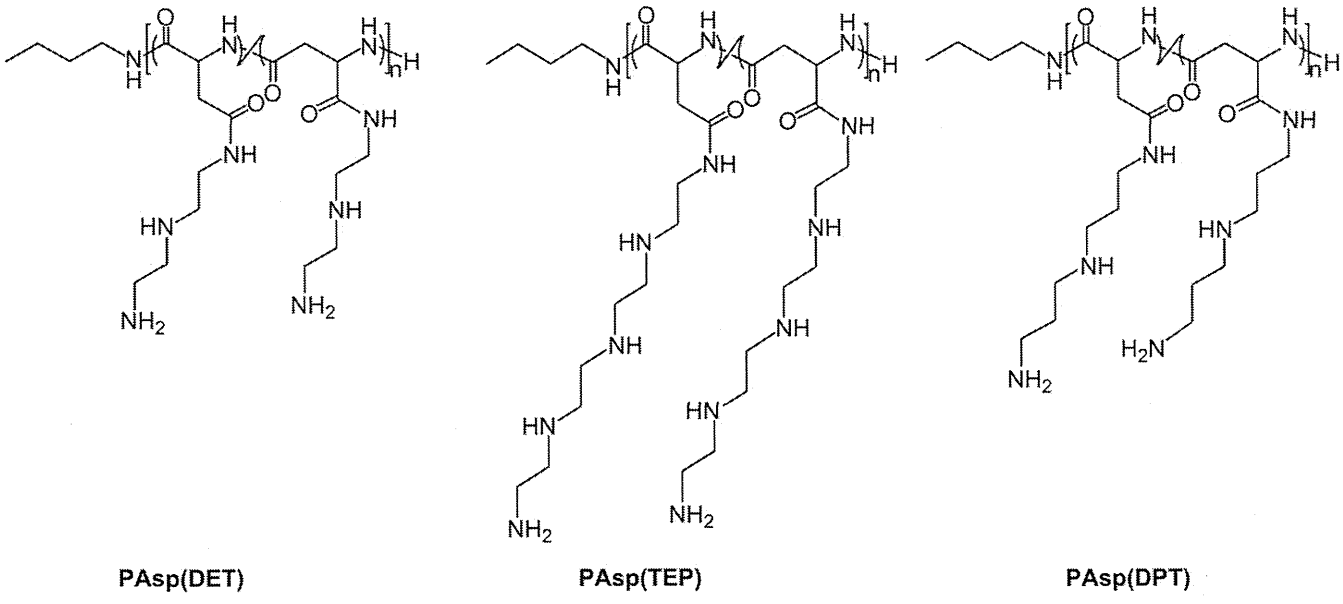

Fig. 1. Chemical structures of PAsp(DET), PAsp(TEP), and PAsp(DPT).

described method [23,24]. The typical synthetic procedure is briefly described for PAsp(DET) as follows. PBLA (DP = 92, 149 mg) was dissolved in NMP (7.5 mL) and cooled to 4 °C. DET (3.9 mL, 50 eq to benzyl groups of PBLA) was diluted with NMP (3.9 mL). The PBLA solution was added dropwise into the DET solution and the mixture stirred for 1 h at 4 °C under an argon atmosphere. Thereafter, the reaction mixture was added dropwise into a cold HCl aqueous solution (0.5 N, 21.8 mL) the temperature of which was kept below 10 °C. The polymer product was purified by dialysis against 0.01 N HCl at 4 °C for one day and then against de-ionized water at 4 °C for 4 h using a dialysis membrane with molecular weight cut off of 6000–8000 Da. The dialyzed solution was lyophilized to obtain the final product (182 mg, yield 91%) as a chloride salt form. PAsp(TEP) and PAsp(DPT) were synthesized in a similar manner; e.g., PBLA (101 mg) and TEP (4.6 mL) to obtain PAsp(TEP) (104 mg, yield 49%), and PBLA (98.9 mg) and DPT (2.8 mL) to obtain PAsp(DPT) (58.7 mg, yield 40%). Each quantitative conversion of PBLA to PAsp(DET), PAsp(TEP), and PAsp(DPT) was confirmed by the ^{1}H NMR spectra in D_2O at 80 °C (data not shown) from the peak intensity ratio of the protons of the butyl group at the α-chain end ($CH_3CH_2CH_2CH_2$-, δ = 0.8–1.5 ppm) to the ethylene protons in the aminoethylene units, i.e., PAsp(DET): $-CONH(CH_2)_2NH(CH_2)_2NH_2$, δ = 3.1–3.5 ppm; PAsp(TEP): $-CONH(CH_2)_2NH(CH_2)_2NH(CH_2)_2NH(CH_2)_2NH_2$, δ = 3.0–3.6 ppm, and to the propylene units in the 1,3-diaminopropane moieties, i.e., PAsp(DPT): $-CONH(CH_2)_3NH(CH_2)_3NH_2$, δ = 1.9–2.1 and δ = 3.1–3.3 ppm.

2.4. Potentiometric titration

PAsp(TEP) (538 mg) was dissolved in 0.1 N HCl (50 mL) containing 150 mM NaCl to adjust residual amine concentration to 100 mM. The titration was conducted with 0.1 N NaOH containing 50 mM NaCl at 37 °C, using an automatic titrator (TS-2000, Hiranuma, Kyoto, Japan). Each titrant (100 μL) was added after the stabilization of pH values (minimal interval: 30 s).

2.5. Preparation of polyion complex (PIC)

Each polyaspartamide derivative dissolved in 10 mM HEPES buffer (pH 7.4) was mixed with 15 μM siRNA solution (10 mM HEPES buffer, pH 7.4) to obtain siRNA-loaded PIC (4 μM siRNA) at the selected mixing ratio (*N*/*P* ratio), which was defined as the residual molar ratio of amines of the polyaspartamide derivatives to phosphates of siRNA. After the incubation for 1 h at 4 °C, the formation of PIC was determined by agarose gel electrophoresis. Each sample solution was loaded into a 1 wt% agarose gel (100 ng siRNA in 5 μl of TAE buffer (pH 7.4)) containing ethidium bromide. After electrophoresis at 100 V for 30 min, the detection was conducted using a Molecular Imager FX (BIO-RAD).

2.6. Dynamic light scattering (DLS) measurement

Size of siRNA-loaded PIC was evaluated by DLS measurements at 25 °C using a Zetasizer Nano-ZS instrument (Malvern Instruments, Malvern, UK) equipped with a He–Ne ion laser (λ = 633 nm). A scattering angle of 173° was used in all measurements. The PICs (*N*/*P* = 10) were prepared at 4 μM siRNA, followed by particle size measurement by DLS.

2.7. Fluorescence correlation spectroscopy (FCS) measurement

A Confocor3 module of LSM 510 (Carl Zeiss, Oberlochen, Germany), equipped with a Zeiss C-Apochromat 40× water objective, was used for FCS analysis. A He–Ne laser (543 nm) was selected for the excitation of Cy3-labeled siRNA and 560–615 nm band-pass filter was selected to filter emission. PICs prepared at 4 μM siRNA (*N*/*P* = 10) were diluted up to 100 nM siRNA with 10 mM HEPES buffer (pH 7.4) or DMEM containing 10% FBS. Each sample was incubated at 37 °C for the set period. Thereafter, 200 μL of samples were put into an 8-well Lab-Tek chambered borosilicate cover-glass (Nalge Nunc International, Rochester, NY) and subjected to FCS analysis (sampling time: 20 s, repeating time: 10). The measured autocorrelation curves were fitted with the Zeiss Confocor3 software to obtain diffusion times, which were then converted to the corresponding diffusion coefficients based on a reference of rhodamine6G. The corresponding diameter of the PICs was further calculated from the Stokes–Einstein equation by assuming a spherical PIC structure [25].

2.8. Luciferase gene silencing assay

B16F10-Luc cells were plated on a 24-well plate at a cell density of 10,000 cells/well in DMEM containing 10% FBS, followed by incubation for 24 h after which the medium was replaced with fresh medium. The PICs loaded with firefly luciferase or scrambled siRNA at *N*/*P* = 10 and 20 were applied at a concentration of 100 nM siRNA. After 48 h incubation, the medium containing siRNA-loaded PIC was removed and cells were washed with 200 μL of PBS, followed by the addition of 200 μL of cell culture lysis buffer (Promega). The expressed luciferase in the lysate was measured using a Luciferase Assay System (Promega) and a luminescence microplate reader (Mithras LB 940, Berthold technologies, Bad Wildbad, Germany). The relative luciferase expression was calculated as a ratio to the expression of non-treated cells. The results were exhibited as a mean and standard deviation of the mean obtained from four samples.

2.9. Cell viability assay

Cell viability was measured using a Cell Counting Kit-8 (Dojindo, Japan). B16F10-Luc cells were plated on a 96-well plate at a cell density of 2500 cells/well in DMEM containing 10% FBS. After incubation for 24 h, the medium was replaced with fresh medium, and siRNA-loaded PICs prepared at *N*/*P* = 10 and 20 were applied at a concentration of 100 nM siRNA. After 48 h incubation, the cell viability was measured following the manufacturer's protocol. The absorbance was measured using a microplate reader equipped with a band-pass filter of 450 nm (Model 680, BIO-RAD, Hercules, CA). The cell viability was determined as a percentage to the absorbance of non-treated cells. The results were expressed as a mean and standard deviation obtained from eight samples.

2.10. Flow cytometric analysis

B16F10-Luc cells were plated on a 6-well plate at a cell density of 50,000 cells/well in DMEM containing 10% FBS, followed by incubation for 24 h. PICs prepared from Cy3-labeled siRNA at *N*/*P* = 10 and 20 were applied to each well at a concentration of 100 nM siRNA. After 12 h of incubation, cells were washed 3 times with 500 μL of PBS, treated by trypsin-EDTA solution, and suspended in PBS. The fluorescence intensity was measured using a BD™ LSR II flow cytometer (BD Biosciences, Franklin Lakes, NJ). The results were expressed as a mean and standard deviation obtained from three samples.

2.11. Confocal laser scanning microscopic (CLSM) analysis

B16F10-Luc cells were plated on a 35 mm glass-based dish (Iwaki, Tokyo, Japan) at a density of 50,000 cells/well in DMEM containing 10% FBS followed by 24 h incubation. The old medium was replaced with fresh medium and each sample prepared from Cy3-labeled siRNA at *N*/*P* = 10 for PAsp(DPT) and 20 for PAsp(TEP) was applied at 100 nM siRNA. After the incubation for 24 h, the staining with LysoTracker Green (Molecular Probes, Eugene, OR) and Hoechst33342 (Dojindo, Japan) was performed, and then the CLSM imaging was conducted using the LSM 510 (Carl Zeiss, Oberlochen, Germany) equipped with a C-Apochromat 63x objective (Carl Zeiss). The excitation wavelengths were 488 nm (Ar laser) for LysoTracker Green, 543 nm (He–Ne laser) for Cy3-labeled siRNA, and 710 nm (MaiTai laser for two photon imaging) for Hoechst33342.

The intracellular distribution of Cy3-siRNA was quantitatively evaluated by calculating the colocalization ratio of Cy3-siRNA with LysoTracker Green as follows:

Colocalization ratio (%) = 100 × [yellow pixels (colocalization of Cy3 with LysoTracker)/yellow and red pixels (all the Cy3 in cells)].

The results were represented as a mean obtained from ten cells.

2.12. Membrane destabilization study

B16F10-Luc cells were plated on a 48-well plate at a cell density of 10,000 cells/well in DMEM containing 10% FBS. After 24 h of incubation, the old medium was removed. The cells were then incubated with 100 μl of PBS (pH 7.4) or 20 mM MES (pH 5.5, 150 mM NaCl) containing PAsp(DET) (5.75 μg/mL), PAsp(TEP) (4.5 μg/mL), or PAsp(DPT) (6.25 μg/mL) for 20 min at 37 °C. The concentration of each polyaspartamide derivative was adjusted to that in the gene silencing assay (*N*/*P* = 10). After washing cells with 1 mL of PBS, 200 μl of PBS containing YO-PRO-1 and Hoechst33342 was added to each well. After 10 min of incubation, the cells were observed with In Cell Analyzer 1000 (GE Healthcare UK Ltd., Buckinghamshire, England). The membrane destabilization activity was determined from the fluorescent intensity of YO-PRO-1 colocalizing with the Hoechst33342 signal. Approximately 3000 cells were analyzed in each well and the results represented as a mean with standard deviation obtained from three wells [26].

3. Results & discussion

3.1. Characterization of cationic polyaspartamide derivatives

Three types of cationic polyaspartamide derivatives possessing the same DP were synthesized by the quantitative aminolysis reaction to flanking benzyl ester groups of PBLA (DP = 92) [27]. Indeed, the successful preparation of PAsp(DET), PAsp(TEP), and PAsp(DPT) (Fig. 1) was confirmed by the ^{1}H NMR measurement (data not shown).

The protonated states of each polyaspartamide derivative at physiological pH of 7.4 and endosomal pH of 5.5 were estimated by the potentiometric titration in 150 mM NaCl solution at 37 °C. Each neutralization point was determined from the differential curves

Table 1
Protonation degree (α) and pKa values of each polyaspartamide derivative.

Polymer	α		pKa_1	pKa_2	pKa_3
	pH 7.4	pH 5.5			
PAsp (DPT)	0.88	0.98	9.7	8.6	
PAsp (TEP)	0.50	0.69	9.0	8.2	6.3
PAsp (DET)	0.53	0.82	9.1	6.3	

obtained from the titration curves (data not shown). The protonation degree (α) and pKa ($= pH + \log[\alpha/(1-\alpha)]$) of each polyaspartamide derivative were calculated and α/pH curves and pKa/α curves created (data not shown). Each pKa value of the flanking amine moieties in the polyaspartamide derivatives was determined from pKa/α curves (Table 1). Note that $pKa_{4,TEP}$ was not obtained here because of the incompletion of the fourth protonation of the *N,N'*-bis(2-aminoethyl)-1,2-diaminoethane unit in PAsp(TEP) even in the lower titration range of pH 1.3. Next, the α of each polyaspartamide derivative at pH 7.4 and 5.5 was determined from the α/pH curves (Table 1). From these values, the major protonated structures of PAsp(DET), PAsp(TEP), and PAsp(DPT) were estimated at pH 7.4 and 5.5 as shown in Fig. 2. PAsp(DET) and PAsp(TEP) bearing one and two 1,2-diaminoethane units, respectively, underwent substantial change in their protonation states of the side chain between pH 7.4 and 5.5: mono-protonated state at pH 7.4 and di-protonated state at pH 5.5 for PAsp(DET); and di-protonated state at pH 7.4 and tri-protonated state at pH 5.5 for PAsp(TEP). In contrast, PAsp(DPT) kept the di-protonated state at both pHs of 7.4 and 5.5. The restricted protonation of PAsp(DET) and PAsp(TEP) at pH 7.4 is reasonably explained by the electrostatic repulsion in di-protonated form of 1,2-diaminoethane unit known as the butane effect (3-bond interaction) [14]. This charge repulsive effect is diminished under 150 mM NaCl condition in 1,3-diaminopropane unit in PAsp(DPT) because of an additional methylene unit between two amino groups, leading to the fully protonation at pH 7.4.

3.2. Physicochemical characterization of siRNA-loaded PICs from cationic polyaspartamide derivatives

The cationic polyaspartamide derivatives (PAsp(DET), PAsp(TEP), and PAsp(DPT)) were applied for PIC preparation with siRNA in 10 mM HEPES buffer (pH 7.4). According to our previous results that PICs prepared at high N/P ratios (>10) showed significant gene silencing efficiency [21,22], the $N/P = 10$ and 20 were selected here for PIC preparation. Agarose gel electrophoresis of the PIC solution revealed that there were no free siRNA bands at both N/P ratios in all the samples examined, indicating the incorporation of all the siRNA molecules into the PICs. Thus, the PICs prepared at $N/P = 10$ and 20 were used for further studies.

Dynamic light scattering (DLS) analysis revealed that the size distribution of PICs (Fig. 3) was highly affected by the side chain structure of the polymers. PAsp(TEP) and PAsp(DPT) allowed the formation of monodispersed siRNA PIC with ~150 nm in size in 10 mM HEPES buffer (pH 7.4). In contrast, the PICs prepared from

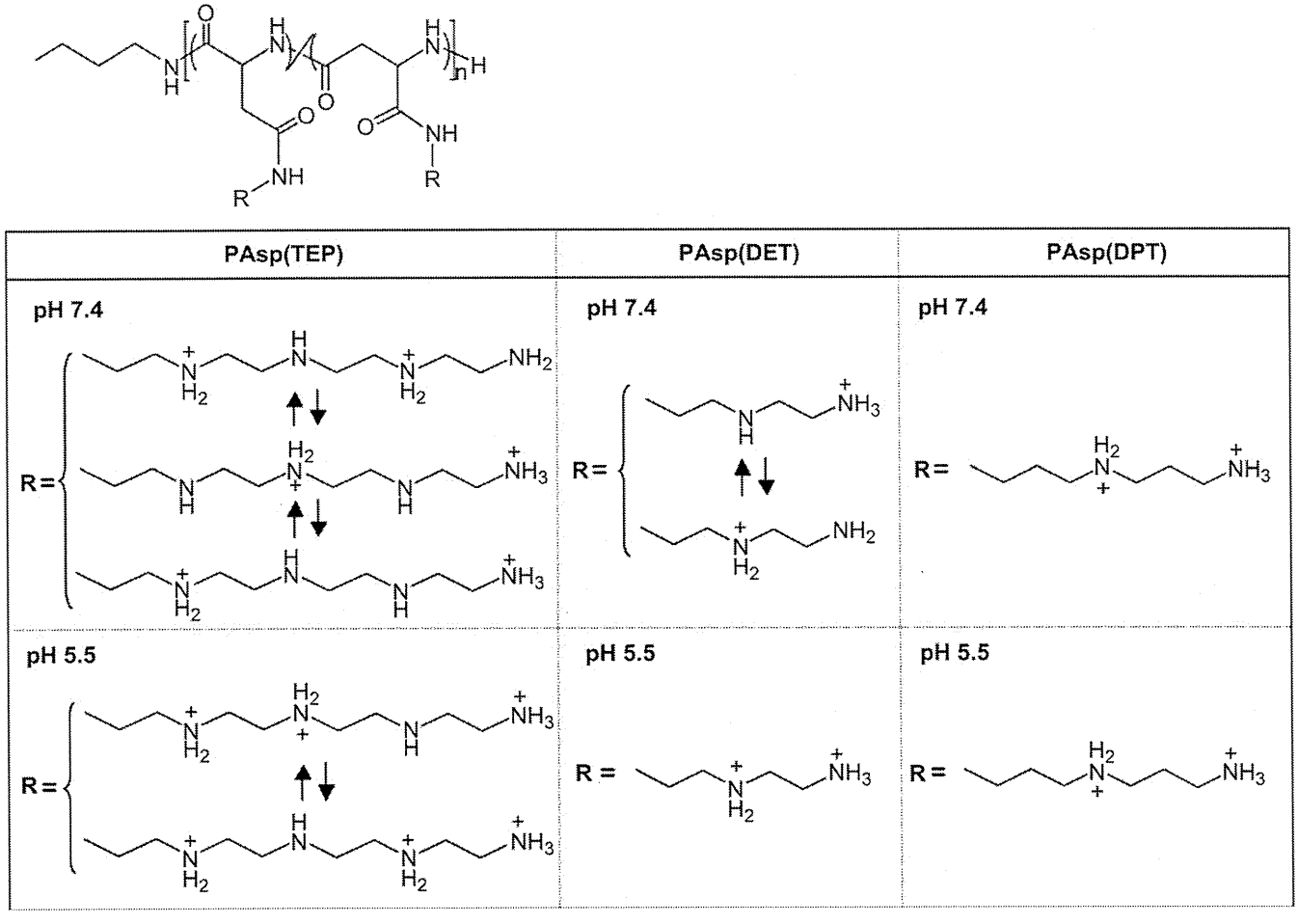

Fig. 2. Major protonated states of PAsp(DET), PAsp(TEP), and PAsp(DPT) at pH 7.4 and pH 5.5, which were estimated from the pKa values.

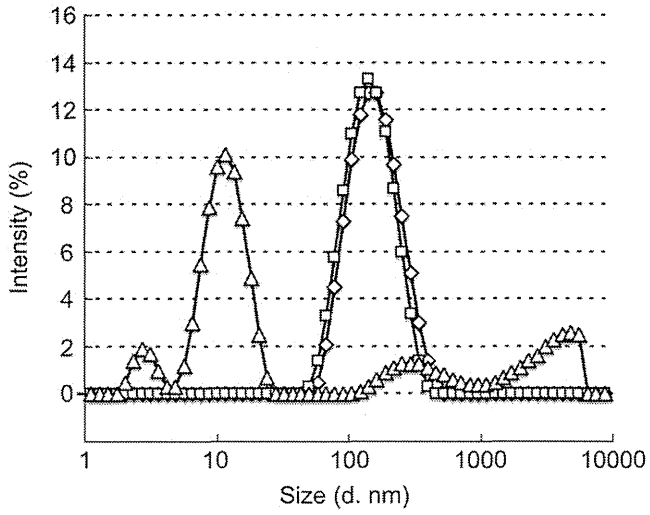

Fig. 3. Size distribution of PICs prepared from the polyaspartamide derivatives at *N/P* = 10 in 10 mM HEPES buffer (pH 7.4) (siRNA: 4 μM). Each symbol represents PAsp(TEP) PIC (open diamond), PAsp(DPT) PIC (open square), and PAsp(DET) PIC (open triangle).

PAsp(DET) had a polydispersed size distribution with a substantially smaller size (~10 nm) as a major fraction in the same buffer. Note that the presence of the small PICs in PAsp(DET) was also observed in the following fluorescence correlation spectroscopy (FCS) analysis (Fig. 4A). These results suggest that higher charge density and the number of protonated amino groups in the side chain may facilitate the formation of PIC particles with narrow size distribution, presumably through the enhanced multivalent interaction with siRNA molecules.

The FCS analysis, which enables the size estimate of fluorescently labeled molecules even in serum-containing media [21,22,28], was conducted to investigate the PIC stability in the cell culture medium containing 10% FBS. Based on the Stokes–Einstein equation with the assumption that PICs prepared were spherical structures, the diffusion coefficients of siRNA-loaded PICs obtained by FCS analysis were converted to the corresponding hydrodynamic radius to obtain the diameter of PICs. siRNA/PAsp(DET) PIC decreased its size to the similar level of naked siRNA molecules (Fig. 4A) within 5 min after the serum addition, indicating the prompt dissociation of the PIC to release free siRNA in the serum-containing medium. In contrast, siRNA/PAsp(TEP) and siRNA/PAsp(DPT) PICs showed no decrease in the size even after 1 h incubation in the serum-containing medium (Fig. 4B), indicating that their PICs were more tolerable in the serum-containing medium. The sizes of these PICs were increased immediately in the serum-containing medium, suggesting the interaction with serum components, most likely anionic serum proteins thereby forming secondary aggregates. The higher charge density and number in the side chain of PAsp(TEP) and PAsp(DPT) are more likely to facilitate a local multivalent binding of the repeating array of positively charged amino groups in the polymer to siRNA phosphates, rendering the PIC tolerable against an exchange with anionic serum proteins.

3.3. Gene silencing study

Gene silencing efficiency of the siRNA-loaded PICs from the cationic polyaspartamide derivatives was examined using B16F10-Luc, a mouse melanoma cell line stably expressing luciferase, by measuring the luciferase luminescence intensity in the cells treated by each PIC after incubation for 48 h (Fig. 5). The significant gene

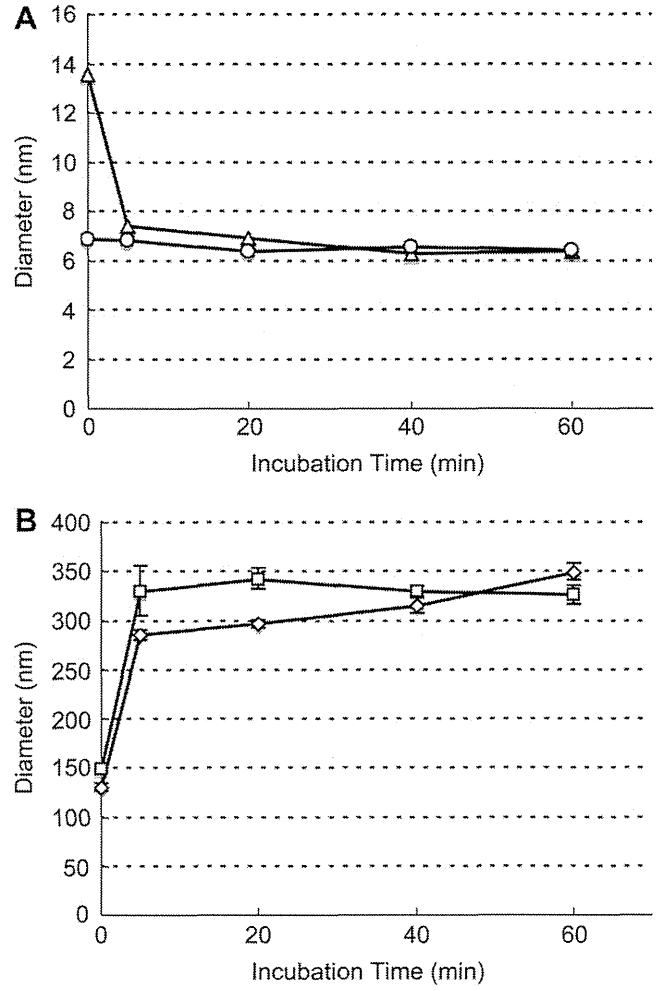

Fig. 4. Time-dependent change in the diameter of (A) PAsp(DET) PIC (open triangle) and naked siRNA (open circle), (B) PAsp(TEP) PIC (open diamond) and PAsp(DPT) PIC (open square) in the cell culture medium (10% FBS). PICs were prepared at *N/P* = 10, and siRNA concentration was set to 100 nM. The diameters were calculated from the diffusion coefficients measured by fluorescence correlation spectroscopy analysis. Results are expressed as the mean ± S.D. (*n* = 10).

silencing was observed in siRNA/PAsp(TEP) PIC at *N/P* = 10 and 20, siRNA/PAsp(DPT) PIC at *N/P* = 10, and ExGen 500 (a linear PEI-based transfection reagent as a control) at *N/P* = 10 and 20, whereas no significant gene silencing was observed for the cells treated by siRNA/PAsp(DET) PIC at *N/P* = 10 and 20. These results were well correlated with the serum tolerability of these PICs. The PICs from PAsp(TEP) and PAsp(DPT) showing high stability in the serum-containing media (Fig. 4) exerted significant gene silencing. Meanwhile, the PAsp(TEP) PICs loaded with scrambled siRNA induced no reduction in the luciferase expression, thus it was confirmed that the decrease in the luciferase expression by PAsp(TEP) PICs with luciferase siRNA was indeed caused by the sequence-dependent gene silencing of siRNA. In contrast, PAsp(DPT) and ExGen 500 PICs with scrambled siRNA resulted in the considerable reduction of luciferase gene expression, especially at *N/P* = 20, due to the severe cytotoxicity of these PICs regardless of siRNA sequence. In fact, a colorimetric cell viability assay revealed the strong cytotoxicity of PAsp(DPT) and ExGen 500 PICs at the higher *N/P* ratio (Fig. 6). Alternatively, PAsp(TEP) induced almost no decrease in the cell viability in this transfection condition, achieving effective gene silencing with negligible cytotoxicity.